Final Report 1999-31

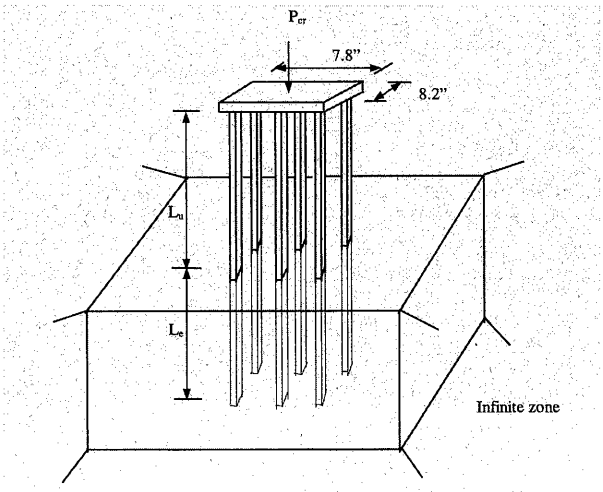

Stability of Pile Groups

Technical Report Documentation Page

1. Report No.	2.	3. Recipient's Accession No.
MN/RC - 1999-31		

4. Title and Subtitle	5. Report Date
STABILITY OF PILE GROUPS	January 1999
	6.

7. Author(s)	8. Performing Organization Report No.
Zhong Zhao Henryk K. Stolarski	

9. Performing Organization Name and Address	10. Project/Task/Work Unit No.
University of Minnesota Department of Civil Engineering 500 Pillsbury Drive, S.E. Minneapolis, MN 55455	11. Contract (C) or Grant (G) No. (C) 74708 TOC # 13

12. Sponsoring Organization Name and Address	13. Type of Report and Period Covered
Minnesota Department of Transportation 395 John Ireland Boulevard St. Paul Minnesota, 55155	Final Report 1999
	14. Sponsoring Agency Code

15. Supplementary Notes

16. Abstract (Limit: 200 words)

Current research focuses on advancing the existing capabilities for stability analysis of pile foundations. To this end, researchers developed a continuum model and a structural model.

In the continuum model, three-dimensional solid finite elements and mapped infinite elements are employed for modeling the three-dimensional geometry, pile-soil-pile interaction, and unbounded domain whereas three-dimensional thin-layer interface elements are used for modeling interaction behavior between the pile and the soil. In contrast, thin-walled structural elements and flat shell elements are used for the piles and pile cap in the structural model. Nonlinear soil springs are adopted for modeling the lateral and axial pile-soil interaction.

The continuum model is capable of accounting for pile-soil interaction and pile-soil-pile interaction appropriately whereas the structural model is efficient and simple to implement. To include pile-soil-pile interaction for groups of closely spaced piles, the group-reduction factor is introduced in an approximate fashion in the structural model. Both the continuum model and structural model developed in the current study are used together for some representative but simpler pile configurations to obtain the group-reduction factor.

17. Document Analysis/Descriptors		18. Availability Statement
Stability analysis Pile foundations	Finite element model	No restrictions. Document available from: National Technical Information Services, Springfield, Virginia 22161

19. Security Class (this report)	20. Security Class (this page)	21. No. of Pages	22. Price
Unclassified	Unclassified	91	

STABILITY OF PILE GROUPS

Final Report

Prepared by

Zhong Zhao
Henryk K. Stolarski
Department of Civil Engineering
University of Minnesota

January 1999

Prepared for

Minnesota Department of Transportation
Office of Research Services
First Floor
395 John Ireland Boulevard, MS 330
St. Paul, MN 55155

ACKNOWLEDGMENT

The authors express their gratitude to the Office of Research Services of the Minnesota Department of Transportation for support of this research. Sincere appreciation is also directed to Dr. Theodore V. Galambos of the Department of Civil Engineering at the University of Minnesota, as well as to Donald Flemming, Gary Peterson, Louis Manjula, Paochen Mma, Rodney Koehn and Rich Lamb of the Minnesota Department of Transportation (Mn/DOT) for useful discussion and feedback provided in the course of the research.

TABLE OF CONTENTS

LIST OF FIGURES

LIST OF TABLES

EXECUTIVE SUMMARY

A study was undertaken to investigate stability of pile groups, with particular emphasis on characteristic features found in bridge foundations. The result of this study is a fairly general computer program, allowing to estimate loads that are critical from the point of view of a given pile foundation. In broad terms, the program allows to trace the large deformation, equilibrium response of the soil/structure system until the critical load is reached. The program is based on the finite element approach. It has been made available to the bridge personnel in the Minnesota Department of Transportation.

There are two main features, distinguishing pile groups in bridge foundations, that had to be incorporated in this study:

1. A possibility of scour. This is accounted for by permitting variations in the scoured and embedded in the soil length of the piles.
2. Interaction of the piles with the remaining part of the structure and with one another. This is included by treating the cap (connecting the piles at the top) as a flexible and inherent part of the analyzed system, and by incorporating the stiffness of the superstructure (which has to be evaluated independently) in the model. The pile cap provides one way the piles interact with one another, the other way is through the soil. To be able to analyze realistic pile groups, which are often large, interaction through the soil is included only in a form of an "interaction factor", also obtained in this study but from a more refined, smaller, model.

There are several specific features included here, which are essential in all pile foundations, including bridge foundations emphasized in this work. Those are:

1. Inclusion of stratified soil configurations. Here the arrangement of soil layers can be specified independently for each pile in the group.
2. Adequate description of the constitutive properties of the soil in each layer. These are included in the form of the force-displacement curves for normal and tangential pile-soil interactions. The curves for the most common soil categories found in the literature are available in the program.
3. Inclusion of thin-wall piles and the corresponding beam theory including warping.
4. Allowing for two types of loads in the systems: those whose critical value is to be established and those that are kept fixed at a specified level during the search for that critical value.

The program developed in the course of this study has been extensively tested. However, considering the lack of the solutions incorporating all of the aspects mentioned earlier, the tests performed had to be limited to some simpler situations. All of them provided results that could be confirmed by an independent analysis. It is therefore believed that the results rendered by the developed computer program are correct. Nevertheless, in view of the uncertainties typically associated with the soil properties, particularly in the severe environment of the bridge foundations, it is advisable to follow the usual rules of a prudent engineering practice. That implies that,

in analyzing critical load for a given foundation, the soil properties should be estimated so as to provide a conservative value of that critical load. With that in mind the program developed here should provide a useful tool, allowing to evaluate effects of many different factors on the integrity of pile foundations. It should be of use both in the analysis of new and in the evaluation of the existing bridges.

CHAPTER 1
INTRODUCTION

The research presented in this report involves practical and academic aspects. From the practical point of view stability of pile groups has to do with design of new and maintenance of the existing bridge structures, one example of which is shown in Fig. 1. Academically, it represents an important part of nonlinear structural analysis, incorporating geometric and material nonlinearities along with computational techniques to trace nonlinear equilibrium path and to detect bifurcation and limit points on that path. Those points relate to stability of the structure.

Stability analysis of pile groups is an inherent ingredient in the design of those new

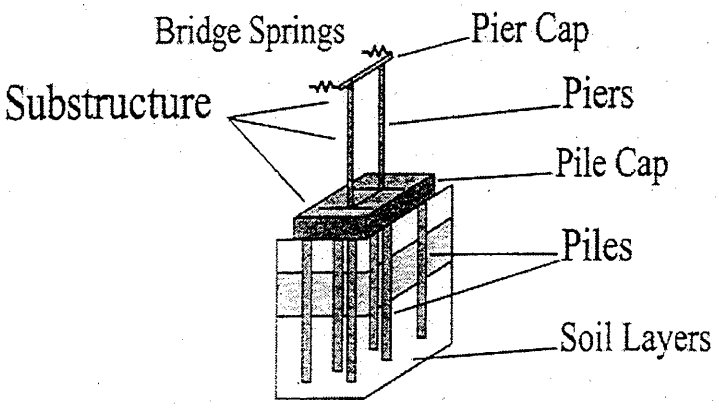

Fig 1.1 Schematic diagram of a bridge structure

(After M.I. Hoit et al [26])

bridge structures in which supporting elements (piers) involve columns (or piles) erected above the level of the soil. Stability of those piers has to be assured to preserve integrity of the bridge.

Relevance of stability analysis in maintenance of the existing bridges has to do with scour. Scour is the erosion of soil from the area surrounding foundation of the bridge piers caused by water. In the case of the bridges whose piers contained columns erected above the original level of the soil, scour changes the exposed length of those columns, changing thereby stability properties of the piers. In the case of the bridges whose original design did not contain columns above the soil level foundation piles can be (and often are) exposed to some extend by scour, which again changes the stability conditions of the pier. Thus, in both cases, the evaluation of the current stability conditions of the scoured bridge foundations must be an integral part of its maintenance.

Analysis of structural stability is nonlinear in its nature, even for problems involving linear elasticity (the corresponding governing equations are obtained by considering large deformation problems first). Stability of pile groups, however, involves some aspects of analysis that go beyond the usual stability analysis of structures, although linear elastic approximation may sometimes provide a valuable information. The main source of the additional difficulties is the interaction of the pile group with the soil (soil-structure interaction), whose realistic description is strongly nonlinear. Not only properties of the soil are nonlinear, but its interaction with the piles has independent nonlinear characteristics, which may influence stability of the pile group even stronger than those of the soil alone.

In view of the complexities outlined in the previous paragraph, which are associated with a realistic description of pile group's stability, analytical solution of the problem seems impossible, unless drastic simplifying assumptions are made. Thus, the present research is focused on numerical solution of the problem.

In this study, a finite element method for three-dimensional analysis of stability of pile groups as a system will be developed. This method will be subsequently used to determine how pile configurations, soil and pile properties, interaction between individual piles in the group and interaction of the piles with the soil affect the stability properties of the pile group.

This report is organized as follows. Chapter 2 provides a review of previous work on pile foundations. Chapter 3 addresses the issues related to computational aspect of stability analysis. A continuum model is presented in chapter 4, and then a structural model is proposed in chapter 5. Finally closure is given in chapter 6.

CHAPTER 2

REVIEW OF PREVIOUS RESEARCH ON PILE FOUNDATIONS

As far as stability of pile groups is concerned, no research done explicitly on that topic has been found in the literature to the best knowledge of the authors.. The research done so far seems to be only concerned with some aspects of stability of single piles. In these studies, the beam resting on Winkler-type elastic foundation was usually adopted as a model of the pile partially embedded in the soil, which is shown in Fig. 2.1

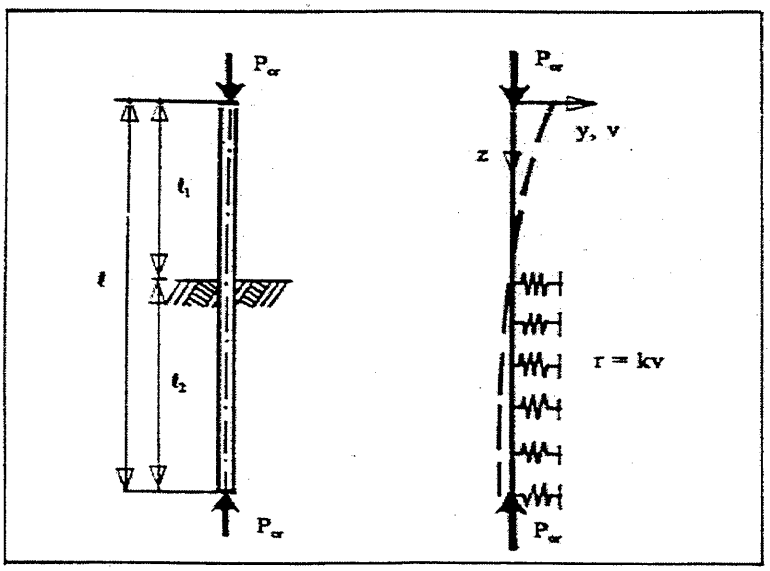

Fig. 2.1 Winkler-type elastic foundation

Brandtzaeg and Harboe [5] and Golder and Skipp [22] used Euler stability theory with the analysis verified using a limited number of buckling tests. Davisson and Robinson [12] presented solutions for buckling loads of partially embedded piles by using the governing differential equation for buckling deflection with the assumptions of

constant axial load on the pile and constant and linearly increasing subgrade moduli. In this case, partially embedded piles were treated as free-standing columns with fixed bases.

Acknowledging the fact that the effect of axial load transfer was neglected in the previous solution, Reddy and Valsangkar [38] investigated this effect by assuming approximate linear and parabolic axial load distributions and by using the energy method. They found that the buckling load was increased considerably due to the change in the load transfer.

Based on a simple one-dimensional idealization of the pile in conjunction with the soil represented by the Winkler-type elastic foundation, Budkowska and Szymczak [7, 8] investigated the sensitivity of the buckling load and initial post buckling equilibrium path of an axially loaded pile partially embedded in the soil. In their research, the effect of the skin friction was neglected and the behavior of the pile-soil system was restricted to linear elastic one.

Gabr and Wang [19] developed a model for estimating the buckling loads of piles assuming uniform variation of the skin friction as a function of depth. In this study, the distribution of the modulus of horizontal subgrade reaction was restricted to the case of linearly increasing with depth. Later on, it was extended to the case of a general power distribution with depth with the use of the minimum potential energy concept [20].

In general, previous work on this subject was conducted in the way that the behavior of the pile-soil system was assumed linear elastic and the effect of soil-pile interaction was not accounted for appropriately.

Current practice of dealing with stability of pile groups is to make some assumptions as to the distribution of the load between individual piles in the system and as to the pile support conditions and then to check if each individual pile is stable or unstable. While this approach provides an estimate of buckling load of the system, it is difficult to establish both the load attributed to each pile and corresponding boundary conditions with sufficient accuracy. Also, this type of modeling does not take into account the fact that due to group action, the behavior of pile groups analyzed as a system may be different from that emerging from independent analysis of individual piles.

There is a substantial amount of publications dealing with other than stability aspects of pile foundations. However, only some of them will be briefly described here.

Adachi and Kimura [1] carried out model pile tests to investigate the interaction factor of the laterally loaded group piles. They found that the interaction factors between each pile were not equal because of the difference in subgrade reaction in front of two piles.

Chow [10] analyzed piles using the modulus of subgrade reaction to model soil response and using the theory of elasticity to consider pile-soil-pile interaction. From his research follows that the design of the piles ignoring group effects may be unduly conservative.

Chen and Poulos [9] performed a simplified boundary-element analysis for piles subjected to lateral soil movements. For their approach the group effect may need to be preassessed via finite element analysis for pile groups.

Using the finite element method, Muqtadir and Desai [34], Selby and Arta [44], Bhowmik [4], Trochanis, Bielak and Christiano [48], and Zaman [53] conducted three-dimensional linear and nonlinear analysis of pile groups.

In dynamic analysis of piles, Dou and Byrne [16], and Kaynia and Mahzooni [29] investigated pile response to earthquake loading. Poskitt [36] calculated the deflection of piles during driving by the use of the theory of elasticity.

With regard to computer programs, Hoit, McVay and others [26] developed a program, called Florida-Pier. This program was designed for the static analysis of bridge pier structures composed of pier columns and cap supported by a pile cap and nonlinear piles with nonlinear soil.

CHAPTER 3

COMPUTATIONAL TECHNIQUE FOR STABILITY PROBLEMS

In stability of pile groups, three types of nonlinearities are involved - geometric nonlinearity, material nonlinearity and nonlinearity due to soil-pile interfaces. In view of the complexity of the problem, the finite element method will be used in the present research. Computationally the key points are associated with the path-following method, detection of stability points and a branch-switching technique between different paths. These issues will be addressed in the sequel.

3.1 PATH-FOLLOWING METHOD

Development of the approximate equations will be followed starting with the nonlinear form of the principle of virtual work

$$\int_{\overset{0}{\Omega}} \underset{\sim}{S} : \delta \underset{\sim}{E}\, d\Omega - \int_{\overset{0}{\Omega}} \rho \underset{\sim}{b} \cdot \delta \underset{\sim}{u}\, d\Omega - \int_{\Gamma_\sigma} \underset{\sim}{t} \cdot \delta \underset{\sim}{u}\, ds = \underset{\sim}{0} \tag{3.1.1}$$

where ρ is the mass density, $\underset{\sim}{b}$ represents the body force, $\underset{\sim}{t}$ denotes the traction vector specified on the part Γ_σ of the boundary $\partial\Omega$, $\underset{\sim}{u}$ is the displacement vector,

$\underset{\sim}{E} = \frac{1}{2}(\underset{\sim}{F}^T \underset{\sim}{F} - \underset{\sim}{I})$ is the Green-Lagrange strain tensor with $\underset{\sim}{F} = \underset{\sim}{I} + \nabla \underset{\sim}{u}$ being the deformation gradient, $\underset{\sim}{S}$ is the 2nd Piola-Kirchhoff stress tensor, $\overset{0}{\Omega}$ represents the domain of the problem, Γ_σ is the boundary with the prescribed traction and symbol δ denotes the variation. In the finite element discretization, we assume

$$\underset{\sim}{u} = \underset{\sim}{N}\,\underset{\sim}{d}$$
$$\underset{\sim}{\delta E} = \underset{\sim}{B}(\underset{\sim}{u})\,\underset{\sim}{\delta d} \tag{3.1.2}$$

in which $\underset{\sim}{N}$ is the matrix of the shape functions, $\underset{\sim}{d}$ is the nodal displacement, $\underset{\sim}{B}$ is the strain-related matrix. The finite element procedure leads to the following form of the basic nonlinear algebraic equilibrium equations

$$\underset{\sim}{G}(\underset{\sim}{u},\lambda) = \underset{\sim}{R}(\underset{\sim}{u}) - \lambda\,\underset{\sim}{P} = \underset{\sim}{0} \tag{3.1.3}$$

where

$$\underset{\sim}{R} = \int_{\overset{0}{\Omega}} \underset{\sim}{B}^{T}\,\underset{\sim}{S}\,d\Omega$$
$$\underset{\sim}{P} = \int_{\overset{0}{\Omega}} \underset{\sim}{N}^{T}\rho\,\underset{\sim}{b}\,d\Omega + \int_{S_\sigma} \underset{\sim}{N}^{T}\,\underset{\sim}{t}\,dS \tag{3.1.4}$$

$\underset{\sim}{R}$ denotes the vector of the internal forces, $\underset{\sim}{P}$ is the vector associated with the pattern of the applied loads, λ represents load parameter. In particular, for elastic processes one has $\underset{\sim}{S} = \underset{\sim}{D}:\underset{\sim}{S}$ *where* $\underset{\sim}{D}$ is a matrix of elastic constants. For other forms of material behavior, $\underset{\sim}{S}(\underset{\sim}{E})$ is more complex.

An arc-length, also called path-following or continuation method by some investigators will be used to trace the equilibrium path described by Eq. (2) to follow both the prebuckling and postbuckling branches. The main idea of continuation methods is to add a single constraint equation to the nonlinear equations (2) [11, 37, 40]. To this end, a special form of an augmented nonlinear system is used

$$\underset{\sim}{\bar{G}}(\underset{\sim}{u},\lambda) = \begin{Bmatrix} \underset{\sim}{G}(\underset{\sim}{u},\lambda) \\ f(\underset{\sim}{u},\lambda) \end{Bmatrix} = \underset{\sim}{0} \tag{3.1.5}$$

where f($\underset{\sim}{u}$,λ) = 0 is a general form of the constraint equation. One example of the constraint equations is given as

$$f(u,\lambda) = (\underset{\sim}{u} - \bar{\underset{\sim}{u}})^T (\underset{\sim}{u} - \bar{\underset{\sim}{u}}) - (\lambda - \bar{\lambda})^2 - c^2 = 0 \tag{3.1.6}$$

where $\bar{\underset{\sim}{u}}, \bar{\lambda}$ are the values of u, λ for the last converged solution, respectively. The consistent linearization of the above given augmented system at a known state u_i *and* λ_i results in the following system of incremental equations

$$\begin{bmatrix} \underset{\sim}{K_T} & -\underset{\sim}{P} \\ \nabla_{\underset{\sim}{u}}{}^T f(\underset{\sim}{u},\lambda) & \nabla_\lambda f(\underset{\sim}{u},\lambda) \end{bmatrix} \begin{Bmatrix} \Delta \underset{\sim}{u} \\ \Delta\lambda \end{Bmatrix}_i = -\begin{Bmatrix} \underset{\sim}{G} \\ f \end{Bmatrix}_i \tag{3.1.7}$$

where K_T is the tangent stiffness matrix, $\nabla_u f$ and ∇_λ are the gradients of the constraint equation (Eq. 3.6) with respect to u and λ, respectively; subscript I represents the ith iteration and ∇u and ∇λ are the increments within the ieration. These equations will be solved by a bordering algorithm [30], which is stated as follows:

Step 1. Solve the two partial equations

$$\Delta v_{Pi} = (K_{Ti})^{-1} P, \qquad \Delta v_{Gi} = -(K_{Ti})^{-1} G_i \tag{3.1.8}$$

Step 2. Calculate the load factor λ

$$\Delta\lambda = -\frac{f_i + f_{vi}{}^T \Delta v_{Gi}}{f_{\lambda i} + f_{vi}{}^T \Delta v_{Pi}} \tag{3.1.9}$$

Step 3. Calculate the total displacement increment

$$\Delta v_i = \Delta\lambda_i \Delta v_{Pi} + \Delta v_{Gi} \tag{3.1.10}$$

Necessary condition for quadratic convergence behavior is the consistent linearization of the constraint equation [43].

It should be noted that the above augmented equations do not provide sufficient information for the purpose of detecting limit and bifurcation points. This observation motivates the use of the extended system of the type considered later.

3.2 COMPUTATION OF STABILITY POINT

3.2.1 Definition of stability points

An equilibrium point is a stability point if the following conditions hold

$$\begin{aligned} &\underset{\sim}{K}_T(\underset{\sim}{\bar{u}}, \bar{\lambda})\,\underset{\sim}{\varphi} = \underset{\sim}{0} \\ &\det \underset{\sim}{K}_T(\underset{\sim}{\bar{u}}, \bar{\lambda}) = 0 \end{aligned} \tag{3.2.1}$$

where $\underset{\sim}{\varphi}$ is the zero eigenvectors of $\underset{\sim}{K}_T$. There are two types of stability points: limit point and bifurcation point. The condition distinguishing limit and bifurcation points is stated as [47]

$$\underset{\sim}{\varphi}^T \underset{\sim}{P} = \begin{cases} = \underset{\sim}{0} & \textit{simple bifurcation point} \\ \neq \underset{\sim}{0} & \textit{limit point} \end{cases} \tag{3.2.2}$$

A main aspect of stability analysis is the detection of stability points. Basically there exist two types of methods for the computation of stability points - indirect and direct methods. With indirect methods [2, 45, 49], the stability points are detected by monitoring a specially computed parameter while the equilibrium path is being traced in a load incremental manner up to the vicinity of those stability points. For example, these

methods may inspect the determinant of the tangent stiffness matrix K_T, the number of negative diagonal elements of K_T [49] or calculate the current stiffness parameter [2]. These methods do not provide any additional information about the stability points beyond identifying their existence. More insight is obtained by using direct methods [50,51,39,45]. In direct methods, a constraint condition which characterizes stability points is included in the system of equations to be solved. These techniques, with a consistent linearization of the extended system, lead to a Newton scheme with quadratic convergence behavior, and the solution of the extended system yields directly the position of the stability points and its associated eigenvector together with the load parameter. In the present research, the following method will be used to directly compute stability points.

3.2.2 Direct computation of stability points

A solution strategy based on the use of following extended system [50]

$$\hat{G}(u, \lambda, \varphi) = \begin{Bmatrix} G(u, \lambda) \\ K_T(u, \lambda)\varphi \\ \varphi \cdot \varphi - 1 \end{Bmatrix} = 0 \qquad (3.2.3)$$

is to be used to compute directly stability points, and provide further information about the nature of these points, which is not readily available in standard solution procedures. The last equation in Eq. (3.10) excludes the trivial solution.

The linearization of the above equations yields the following system of equations

$$\begin{bmatrix} \underset{\sim}{K_T} & \underset{\sim}{0} & -\underset{\sim}{P} \\ \nabla_u(\underset{\sim}{K_T}\,\underset{\sim}{\varphi}) & \underset{\sim}{K_T} & \nabla_\lambda(\underset{\sim}{K_T}\,\underset{\sim}{\varphi}) \\ \underset{\sim}{0} & \underset{\sim}{\varphi}^T/\|\underset{\sim}{\varphi}\| & 0 \end{bmatrix} \begin{Bmatrix} \Delta \underset{\sim}{u} \\ \Delta \underset{\sim}{\varphi} \\ \Delta\lambda \end{Bmatrix} = -\begin{Bmatrix} \underset{\sim}{G}(\underset{\sim}{u},\lambda) \\ \underset{\sim}{K_T}(\underset{\sim}{u},\lambda) \\ \|\underset{\sim}{\varphi}-1\| \end{Bmatrix} \tag{3.2.4}$$

Using a block elimination technique a solution scheme of the above equations can be developed which needs only one factorization of the tangent stiffness [50] and is shown below.

Step 1. Solve

$$K_T \Delta v_P = P, \qquad K_T \Delta v_G = -G \tag{3.2.5}$$

Step 2. Compute within a loop over all elements

$$\begin{aligned} h_P &= \nabla_v(K_T\varphi)\Delta v_P + \nabla_\lambda(K_T\varphi), \\ h_G &= K_T\varphi + \nabla_v(K_T\varphi)\Delta v_G \end{aligned} \tag{3.2.6}$$

Step 3. Solve

$$K_T \Delta\varphi_P = -h_P, \qquad K_T \Delta\varphi_G = -h_G \tag{3.2.7}$$

Step 4. Compute new increments

$$\begin{aligned} \Delta\lambda &= \frac{-\varphi^T \Delta\varphi_G - \|\varphi\|^2 + \|\varphi\|}{\varphi^T \Delta v_P} \\ \Delta v &= \Delta\lambda \Delta v_P + \Delta v_G \\ \Delta\varphi &= \Delta\lambda \Delta\varphi_P + \Delta v_G \end{aligned} \tag{3.2.8}$$

3.3 CALCULATION OF SECONDARY BRANCHES

To calculate the number of existing branches, the associated eigenvalue problem has to be solved near stability points. The number of possible branches in a bifurcation point is determined by the number of zero eigenvalues ω_j. The eigenvectors φ_j indicate the direction of the solution to be followed for the calculation of a secondary branch associated with $\omega_j=0$.

A simple but effective engineering approach is to perturb the equilibrium state in a singular point by these eigenvectors [49]. This perturbation is performed by adding the scaled eigenvector to the deformed configuration in the following way

$$u_j = \bar{u} + \xi_j \frac{\varphi_j}{\|\varphi_j\|} \tag{3.3.1}$$

u_j denotes the perturbed deformed configuration which is used as starting vector for branch switching. $\bar{u}$ is the displacement vector of the last converged solution and φ_j is the j-th eigenvector. ξ_j denotes a scaling factor which is critical for a successful branch switching [49].

Once a secondary branch is reached a further path-following can be done using a standard arc-length scheme.

CHAPTER 4
CONTINUUM MODEL

In the formulation of the problem, the essential issues include modeling of discontinuous behavior at the soil-pile interface and modeling of far-field soil medium. In the present study, a three-dimensional continuum model is proposed to conduct stability analysis of pile groups. In this model, piles, cap, and near-field soil medium are modeled using three-dimensional solid finite elements whereas far-field soil medium modeled using mapped infinite elements. Particularly, three-dimensional thin-layer interface elements are used to model soil-pile interaction. The related issues will be discussed in the following.

4.1 NONLINEAR FINITE ELEMENT FORMULATION FOR SOLIDS

From the nonlinear form of the principle of virtual work, one can obtain the tangent stiffness matrix:

$$\underset{\sim}{K_T} = \frac{\partial \underset{\sim}{R}}{\partial \underset{\sim}{d}} = \underset{\sim}{K_m} + \underset{\sim}{K_g} \tag{4.1.1}$$

where R is the internal force vector, $\underset{\sim}{K_m}$ is the material part and $\underset{\sim}{K_g}$ is the geometrical part of the stiffness matrix K_T. In more detail, the Green-Lagrange strain $\underset{\sim}{E}$ can be expressed as

$$\underset{\sim}{E} = \underset{\sim}{E}_0 + \underset{\sim}{E}_L = \begin{Bmatrix} \varepsilon_x \\ \varepsilon_y \\ \varepsilon_z \\ \gamma_{xz} \\ \gamma_{yz} \\ \gamma_{xy} \end{Bmatrix} = \begin{Bmatrix} u_{,v} \\ v_y \\ w_z \\ v_z + w_y \\ w_x + u_z \\ u_y + v_x \end{Bmatrix} + \frac{1}{2} \begin{Bmatrix} r_x' \underset{\sim}{r}_x \\ r_y' \underset{\sim}{r}_y \\ r_z' \underset{\sim}{r}_z \\ r_z' \underset{\sim}{r}_y + r_y' \underset{\sim}{r}_z \\ r_z' \underset{\sim}{r}_x + r_x' \underset{\sim}{r}_z \\ r_y' \underset{\sim}{r}_x + r_x' \underset{\sim}{r}_y \end{Bmatrix} \tag{4.1.2}$$

where

$$\begin{aligned} r_x' &= \{u_{,x} \quad v_{,x} \quad w_{,x}\} \\ r_y' &= \{u_{,y} \quad v_{,y} \quad w_{,y}\} \\ r_z' &= \{u_{,z} \quad v_{,z} \quad w_{,z}\} \end{aligned} \tag{4.1.3}$$

Further, one has

$$\underset{\sim}{E}_L = \frac{1}{2} \begin{bmatrix} r_x^T & 0 & 0 \\ 0 & r_y^T & 0 \\ 0 & 0 & r_z^T \\ 0 & r_z^T & r_y^T \\ r_z^T & 0 & r_x^T \\ r_y^T & r_x^T & 0 \end{bmatrix} \begin{Bmatrix} r_x \\ r_y \\ r_z \end{Bmatrix} = \frac{1}{2} A r \tag{4.1.4}$$

And

$$\delta \underset{\sim}{E}_L = \frac{1}{2} A \delta r + \frac{1}{2} \delta A r \tag{4.1.5}$$

Vector $\underset{\sim}{r}$ can be expressed in terms of $\underset{\sim}{d}$ if approximation given in Eq. 3.1.2 is taken into account.

$$\underset{\sim}{r} = \underset{\sim}{G}\,\underset{\sim}{d} \tag{4.1.6}$$

where G is a constant matrix. Consequently,

$$\delta\underset{\sim}{r} = \underset{\sim}{G}\,\delta\underset{\sim}{d} \tag{4.1.7}$$

Furthermore, since

$$(\delta\underset{\sim}{A})\underset{\sim}{r} = \underset{\sim}{A}\,\delta\underset{\sim}{r} \tag{4.1.8}$$

one obtains

$$\delta\underset{\sim}{E}_L = (\underset{\sim}{A}\underset{\sim}{G})\delta\underset{\sim}{d} = \underset{\sim}{B}_L\,\delta\underset{\sim}{d} \tag{4.1.9}$$

and

$$\delta\underset{\sim}{E} = \delta\underset{\sim}{E}_0 + \delta\underset{\sim}{E}_L = (\underset{\sim}{B}_0 + \underset{\sim}{B}_L)\delta\underset{\sim}{d} = \underset{\sim}{B}\,\delta\underset{\sim}{d} \tag{4.1.10}$$

$$\underset{\sim}{B} = \underset{\sim}{B}_0 + \underset{\sim}{B}_L \tag{4.1.11}$$

Considering that G is a constant matrix, the following holds

$$\delta\underset{\sim}{B}_L = \delta\,\underset{\sim}{A}\underset{\sim}{G} \tag{4.1.12}$$

With the proceeding notation the variation of the residual R of Eq. 3.1.4 can be written as

$$\delta \underset{\sim}{R} = \int_{\Omega} (\delta \underset{\sim}{B}^T \underset{\sim}{S} + \underset{\sim}{B}^T \delta \underset{\sim}{S}) d\Omega \tag{4.1.13}$$

Recognizing the earlier expression defining $\delta \underset{\sim}{B}$ and the fact that $\delta \underset{\sim}{S} = \underset{\sim}{D} \underset{\sim}{B} \delta \underset{\sim}{d}$, one obtains

$$\delta \underset{\sim}{R} = (\underset{\sim}{K}_m + \underset{\sim}{K}_g) \delta \underset{\sim}{d} = \underset{\sim}{K} \delta \underset{\sim}{d} \tag{4.1.14}$$

Therefore, the material part is given as

$$\underset{\sim}{K}_m = \int_{\Omega} \underset{\sim}{B}^T \underset{\sim}{D} \underset{\sim}{B} dV \tag{4.1.15}$$

As for the geometrical part, one has

$$\underset{\sim}{K}_g \delta \underset{\sim}{d} = \int_V \delta \underset{\sim}{B}_L{}^T \underset{\sim}{S} dV = \int_V \underset{\sim}{G}^T \delta \underset{\sim}{A}^T \underset{\sim}{S} dV = \int_V \underset{\sim}{G}^T \underset{\sim}{M} \delta \underset{\sim}{r} dV = (\int_V \underset{\sim}{G}^T \underset{\sim}{M} \underset{\sim}{G} dV) \delta \underset{\sim}{d} \tag{4.1.16}$$

This gives the expression of the geometrical part

$$\underset{\sim}{K}_g = \int_V \underset{\sim}{G}^T \underset{\sim}{M} \underset{\sim}{G} dV \tag{4.1.17}$$

where

$$\underset{\sim}{M} = \begin{bmatrix} S_x \underset{\sim}{I}_3 & S_{xy} \underset{\sim}{I}_3 & S_{xz} \underset{\sim}{I}_3 \\ S_{xy} \underset{\sim}{I}_3 & S_y \underset{\sim}{I}_3 & S_{yz} \underset{\sim}{I}_3 \\ S_{xz} \underset{\sim}{I}_3 & S_{yz} \underset{\sim}{I}_3 & S_x \underset{\sim}{I}_3 \end{bmatrix} \tag{4.1.18}$$

4.2 SOIL-PILE INTERFACE MODEL

Soil-structure interaction plays an important role in the stability of pile groups. A couple of interface models have been proposed in the literature to model discontinuous behavior at the soil-structure interface. These include:

(a) Thin 2D finite elements with standard constitutive laws [24,35];

(b) Linkage elements in which only the opposite nodes are connected. Usually opposite nodes are connected by discrete springs [18,25];

(c) Special interface elements of either zero or finite thickness [13,14,21,23,27,31,52];

(d) Hybrid methods where the soil and structure are modeled separately and linked via constraint equations to maintain compatibility at the interface [28,32,42].

Among these methods, the interface element method has attracted considerable attention and has been used to solve a lot of soil-structure interaction problems. There exist two types of interface elements, that is, zero-thickness [13,21,23] and thin-layer elements [14,52,27].

Zero-thickness elements are derived on the basis of relative nodal displacements of the solid elements surrounding the interface element. For 2-D analysis, the stress-relative displacement relation is expressed as

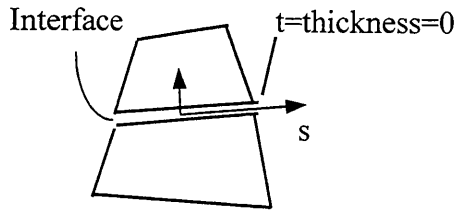

$$\begin{Bmatrix} \sigma_n \\ \tau \end{Bmatrix} = \begin{bmatrix} K_n & 0 \\ 0 & K_s \end{bmatrix} \begin{Bmatrix} v_r \\ u_r \end{Bmatrix} \tag{4.2.1}$$

where K_n and K_s are normal and shear stiffness, v_r and u_r are relative normal and shear displacements. In most zero-thickness elements, the shear behavior is simulated as nonlinear elastic, and a high value is assigned for the normal stiffness based on the assumption that the structural and geological media do not overlap at interfaces. However the use of such arbitrarily high value may not be appropriate. Generally speaking, the formulation can provide satisfactory solutions for the stick and slip deformation modes for which the normal stress remains compressive. For other modes such as debonding, the solutions are often unreliable. On the other hand, it is difficult to incorporate relative dof's into a finite element program. This formulation also causes problems at joint interactions.

The thin-layer element is treated essentially like a solid element, but with different constitutive properties

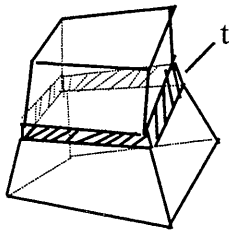

$$d\underset{\sim}{\sigma} = \begin{bmatrix} C_{nn} & C_{ns} \\ C_{sn} & C_{ss} \end{bmatrix} d\underset{\sim}{\varepsilon} \qquad (4.2.2)$$

where C_{nn} = normal component, C_{ss} = shear component, C_{sn} and C_{ns} represent coupling effects. A basic assumption is that the behavior near the interface involves a finite thin zone, rather than a zero thickness as in zero-thickness elements. The thin-layer interface elements have been derived by assuming them to be linear elastic, nonlinear elastic or elastic-plastic. Depending on the material models used, criteria such as Mohr-Columb and Drucker-Prager were used to define the initiation of slip at the interface. For thin-layer interface elements, choice of element thickness is very important. If it is too small,

computational difficulties may arise. For example, solutions would lock up and there would be stress oscillations in the interface elements, and therefore the stress in the adjacent 2D elements is often adopted rather than the interface element stress itself. The latter problem was also encountered by zero-thickness elements. Thus, one has to perform parametric studies in which the predictions from various thickness are compared with observations in order to resolve the question. It has been recommended [14] that the aspect ratio t/L should be in the range of 0.1 to 0.01. But they may vary with different constitutive models. Another shortcoming of existing interface elements is that the behavior of the element would be sensitive to the geometric distortion of the element.

In comparison with zero-thickness elements, thin-layer elements are computationally more reliable because it is capable of providing improved definition of normal and shear behavior; they are easier to program and implement. In addition, inclusion of a finite thickness for the interface can be realistic since there is very often a thin layer of soil, which participates in the interaction behavior. To some degree a zero-thickness element may be viewed as a limiting case of a thin-layer element as its thickness approaches zero.

In the present study, thin-layer interface elements will be used based on the constitutive model by Zaman et al [52]. The tangent shear modulus G_i of the interface is defined as

$$G_i = \partial\tau^0 / \partial\theta \qquad (4.2.3)$$

where $\theta = u_r^0/t$ is the shear strain, u_r^0 is the relative shear displacement, t is the thickness of the interface element. Further a polynomial form is used for τ^0

$$\tau^0 = \alpha_1 + \alpha_2 u_r^0 + \alpha_3 (u_r^0)^2 \qquad (4.2.4)$$

where α_i are interface parameters. For some soil types, these parameters have been reported in [52].

With such interface elements various modes of deformation, including stick or no slip, slip, debonding and rebonding, shown in Fig. 4.2.1, can be simulated by using appropriate stress redistribution scheme as follows.

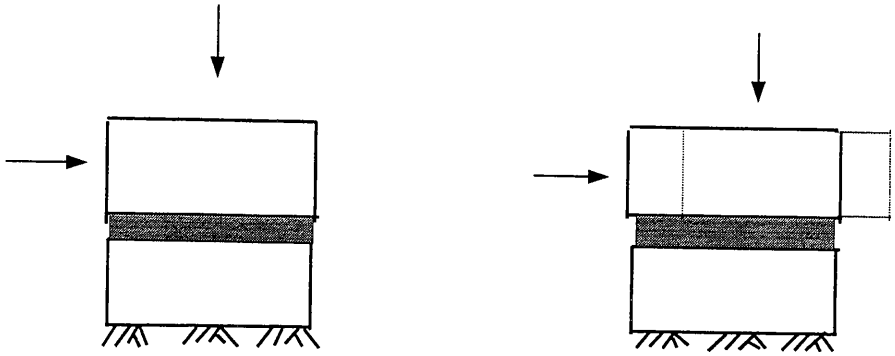

(a) Stick or no slip

(b) Slip

(c) Debonding

(d) Rebonding

Fig. 4.2.1 Deformation modes of an interface

Assume that the previous mode is in stick mode and the values of σ^0_n, τ^0_n, and u^0_n are known at time t and trial response is $\Delta\sigma_n$, $\Delta\tau$ and Δu_n. The element will stay in stick mode if

$(\sigma^0_n+\Delta\sigma) >0$ (compressive), and

$F_s(\sigma^0_n+\Delta\sigma, \tau^0+\Delta\tau) = (sgn) \{(\tau^0 + \Delta\tau\} - [C_a +\{\sigma^0_n + \Delta\sigma_n\}\tan\alpha] < 0$

where

C_a = the activated adhesion,

α = the activated friction angle,

sgn = 1 if $(\tau^0 + \Delta\tau) > 0$

= -1 if $(\tau^0 + \Delta\tau) < 0$

F_s is called a slip function and shown in Fig. 4.2.2.

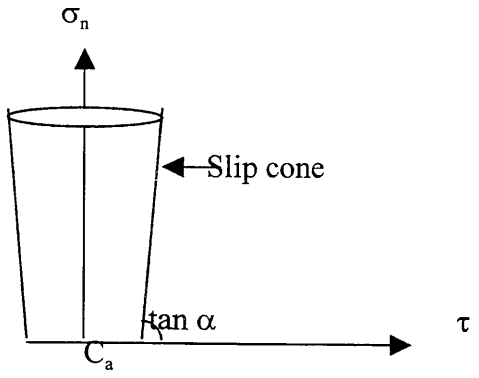

Fig. 4.2.2 Graphical representation of Slip function F_s

The element goes into slip mode if

$(\sigma^0_n+\Delta\sigma_n) >0$ (compressive), and

$F_s(\sigma+\Delta\sigma, \tau+\Delta\tau) \geq 0$

In this case, iterations are performed within the time step, until $F_s \approx 0$ is satisfied. At each iteration, the residual value of F_s is converted into forces and applied to the system as self-equilibrating nodal loads.

The element goes into debonding mode if

$$(\sigma^0_n + \Delta\sigma_n) < 0 \text{ (tensile)}$$

Assuming that for an element in the separation mode,

$$\sigma^0_n + \Delta\sigma_n = R_1,$$

$$\tau^0 + \Delta\tau = R_2.$$

Iterations are performed in such a way that R_1 and R_2 are converted into self -equilibrating nodal loads that are applied to the system during the iterative corrections.

The element is said to be in rebonding mode if

$$(\sigma^0_n + \Delta\sigma_n) > 0 \text{ (compressive), and}$$

$$F_s(\sigma^0_n + \Delta\sigma_n, \tau^0 + \Delta\tau) < 0$$

Approximately, full contact over an element is assumed during rebonding.

4.3 MAPPED INFINITE ELEMENT

One of difficulties in the analysis of soil-structure interaction problems is caused by the semi-infinite nature of the underlying soil media. Several techniques have been used to treat unbounded domain problems with some success.

The boundary element method is very attractive in modeling the exterior of unbounded problems [6, 54]. However, the boundary element method lacks the bandedness and symmetry of the resulting coefficient matrices. In addition material and geometric nonlinearities are difficult to handle using the boundary element method.

Use of the infinite element is another technique for the solution of the far-field problems. For infinite elements in which an exponential and/or reciprocal decay function was employed [3, 17], modified Gauss-Laguerre coordinates of integration points and weights had to be used. In addition, since the exponential decay infinite elements used a decay parameter whose selection is usually problem-dependent, they were not suitable for implementation in general purpose code.

Recently a type of mapped infinite element has been widely used [55,33], based on the mapping of an infinite region into a finite one using appropriate transformation. The implementation of the elements is simple and they retain the standard integration points and weights, making it convenient for coupling with standard FE formulation and for implementation in a general purpose code. This type of mapped infinite elements will be applied to 3-D pile-soil interaction problems.

Consider first the one-dimensional three-node infinite element shown in Fig. 4.3.1, where node 3 is placed at infinity. On that figure h represents distance between node 1 and 2 and x_0 location of the origin of the new coordinate r that, for convenience, is

introduced in the sequel The transformation from the local coordinate $\xi \in (-1, 1)$ to the global coordinate x

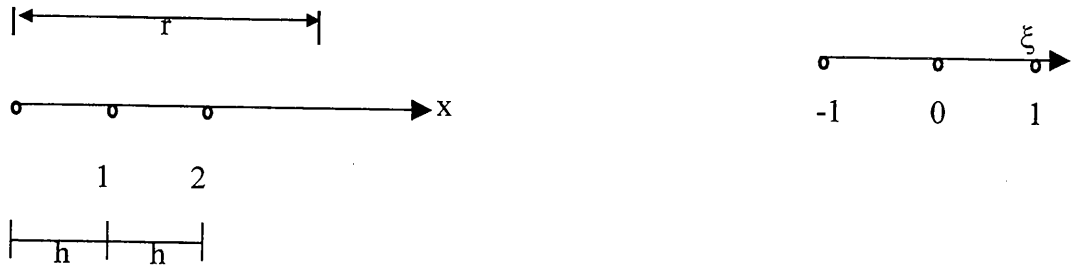

Fig.4.3.1 Mapping of an one-dimensional infinite element

can be written as

$$x(\xi) = \sum_{i=1}^{2} M_i(\xi) x_i \qquad -1 \le \xi \le 1 \tag{4.3.1}$$

where M_i are the mapping functions,

$$M_1(\xi) = -\frac{2\xi}{1-\xi}$$

$$M_2(\xi) = 1 - M_1(\xi) \tag{4.3.2}$$

Note that ξ=-1, 0 and 1 correspond to nodal positions, $x = x_1, x_2$ *and* ∞, respectively in the global coordinate system. The unknown variable displacement u in this case may be interpolated through standard shape functions which, for the three-node element discussed here, can be expressed as

$$u = u_1 N_1 + u_2 N_2 = u_1 \frac{1}{2}\xi(-1+\xi) + u_2(1-\xi) \tag{4.3.3}$$

Considering that ξ=1-2h/r, which is obtained by solving Eq. (4.3.1) for ξ and introducing a new coordinate $r = x + 2h - x_2$ (see Fig. 4.3.1), the above equation can be transformed to

$$u = (4u_2 - u_1)(h/r) + 2(u_1 - 2u_2)(h/r)^2 \tag{4.3.4}$$

which implies that u vanishes at infinity, which is the case for pile-soil interaction problems.

For 3-D problems, the mapping is achieved by products of the shape functions. For example, if the element is infinite in η direction, the one-dimensional mapping functions discussed above are used in the direction (η) and the standard Lagrange shape functions are used in the finite directions (ξ, and ζ). Thus, for a 16- node infinite element (Fig.4.3.2) to be used for matching the 20-node elements used for soil, we have

$$x(\xi,\eta,\zeta) = \sum_{I=1}^{16} \overline{M}_I(\xi,\eta,\zeta)x_I$$

$$\overline{M_i} = \begin{cases} N_i(\xi,\zeta) * M_1(\eta) & i = 1,2,...8 \\ N_{i-8}(\xi,\zeta) * M_2(\eta) & i = 9,10,..16 \end{cases} \tag{4.3.5}$$

where N_i are standard 8-node Serendipity shape functions.

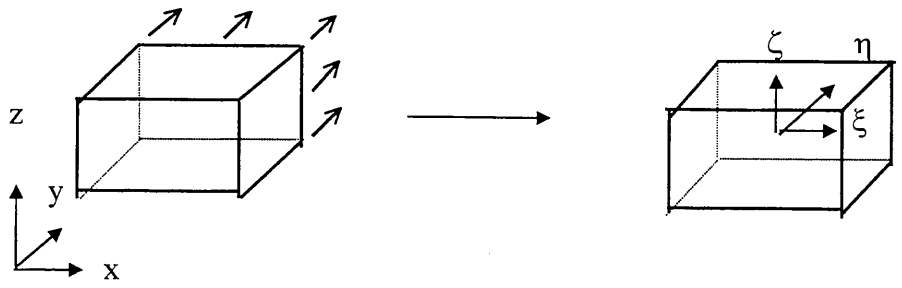

Fig. 4.3.2 Three-dimensional infinite element with η corresponding to infinite direction

In deriving the infinite element equations, the unknown variables are expressed in terms of the standard shape function $\overline{N_I}$,

$$u(\xi,\eta,\zeta) = \sum_{I=1}^{16} \overline{N_I}(\xi,\eta,\zeta) u_I \tag{4.3.6}$$

For an implementation of the mapped infinite element in an existing FE program, it is necessary to compute only the transformations for mapping the infinite region into a finite one and the corresponding Jacobean of these transformations. The remaining procedure is similar to that followed in a standard FE program.

4.4 CONSTITUTIVE MODELS FOR SOIL

Several advanced constitutive laws for soil have been developed [46]. In the present study, the widely used linear elastic, Drucker-Prager, critical state and cap models is implemented in three-dimensional analysis. Brief descriptions of these constitutive models are presented in the following. For detailed information. The reader is referred to the appropriate literature cited in the following.

4.4.1 Drucker-Prager Model [58]

The Drucker-Prager yield critirion is expressed as

$$F = \sqrt{J_{2D}} - \alpha J_1 - K = 0 \tag{4.4.1}$$

where α and K are positive material parameters.

4.4.2 Critical State Model [41]

For both critical state and cap models, there are two yield surfaces associated with material behavior. The failure surface, F_f, is fixed in position, whereas the cap surface F_c can expand or contract depending on the hardening behavior, which is shown in Fig. 4.4.1.

For the modified cam clay model which is one of the critical models, the failure surface F_f and the cap surface F_c have been obtained as

$$F_f = q - Mp \tag{4.4.2}$$

and

$$F_c = q^2 - M^2 pp_0 + M^2 p^2 \tag{4.4.3}$$

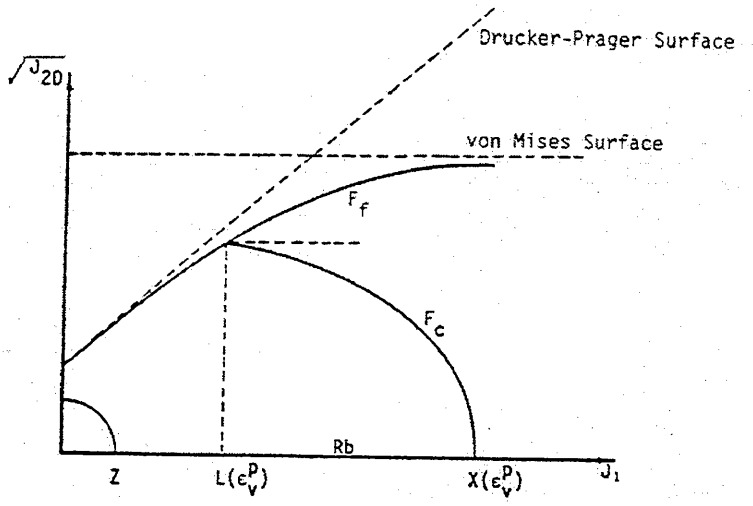

Fig. 4.4.1 Failure and cap surfaces

where $q = (\sigma_1 - \sigma_3) = \sqrt{3J_{2D}}$, and $p = (\sigma_1 + 2\sigma_3)/3 = (\sigma_1 + \sigma_2 + \sigma_3)/3 = J_1/3$, and p_0 is the hardening parameter, which is the intercept of current yield surface with mean pressure axis. The quantities q and p are defined with respect to a cylindrical triaxial device where $\sigma_2 = \sigma_3$. The plastic stress-strain behavior can be described with three parameters, M, λ_c and κ where M is the slope of critical state line on q-p plot, λ_c is the slope of loading path on e-lnp plot and κ is the slope of unloading-reloading path on the same plot.

4.4.3 Cap Model [15]

In this model the failure surface and cap surface are given as

$$F_f(J_1, \sqrt{J_{2D}}) = \sqrt{J_{2D}} - [\alpha - \gamma \exp(-\beta J_1)] = 0 \qquad (4.4.4)$$

and

$$F_c(J_1, \sqrt{J_{2D}}, \varepsilon_v^p) = R^2 J_{2D} - (X - L)^2 + (J_1 - L)^2 = 0 \qquad (4.4.5)$$

where α, β, and γ are material parameters, $X(\varepsilon_v^p)$ and $L(\varepsilon_v^p)$ refer to geometric properties of the elliptic yield surface, Fig. 4.4.1. It is assumed that the ratio R, of major to minor axes remains the same for all ellipses. The quantity X can be related to the hardening parameter ε_v^p as

$$\varepsilon_v^p = W[1 - \exp(-DX)] \qquad (4.4.6)$$

and

$$X(\varepsilon_v^p) = L(\varepsilon_v^p) + R[\alpha - \gamma \exp\{-\beta L(\varepsilon_v^p)\}] \qquad (4.4.7)$$

where D and W are material parameters.

4. 5 RESULTS AND DISCUSSIONS FOR CONTINUUM MODEL

The continuum model for stability of pile groups developed in the previous sections has been implemented and used to solve several example problems in which the section of the piles is a square of 0.4(in.)x0.4(in.) or 0.8 (in.)x0.8 (in.). In the following computations, pile cap, piles and near-field soil medium are modeled by three-dimensional 20-noded elements, whereas the far-field soil medium is modeled by 16-noded mapped infinite elements. Three-dimensional 20-noded interface elements are used for the modeling of the soil-pile interaction. The behavior of piles and pile cap is assumed linearly elastic. The values of the elastic modulus and Possion ratio used are $E_P=10^7$(Psi), $\nu_P = 0.2$ for pile cap and piles. The material parameters for soil are $E_S = 7x10^4$(Psi), ν_S =0.3, cohesion c= 3.5 psi and friction angle $\Phi = 30^0$. For the soil-pile interface, the following interface parameters: $\alpha_1 = 0.0$, α_2=1300.0, and α_3 = -2500.0 are used in Eq. 4.2.4. All the units are in lb. and in.

4.5.1 Single Pile

This problem was used to verify the FE model by comparing with the well-known Euler's buckling load for a free-fixed column shown in Fig. 4.5.1. The details of the single pile and schematic diagram of the finite element mesh for the section A-A are given in Fig. 4.5.2 and 4.5.3, respectively. The buckling loads obtained by assuming a very stiff soil to model fixed end is P_{cr} = 8508 (lb), which is very close to the Euler's solution $P_{cr} = \pi^2EI/4L_u^2$ = 8422 (lb) for the free-fixed column. The difference is due to the approximation error of the finite element method. When the reasonable property of soil

given above was used, the finite element solutions were obtained as P_{cr} = 6228 (lb) (without the use of interface elements) and P_{cr} =5112 (lb) (with the use of interface elements). It is seen that the effect of interface is significant.

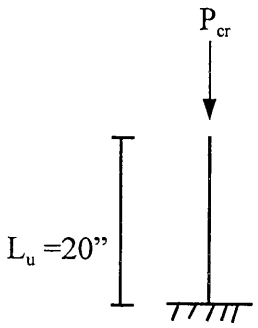

Fig. 4.5.1 Free-fixed column

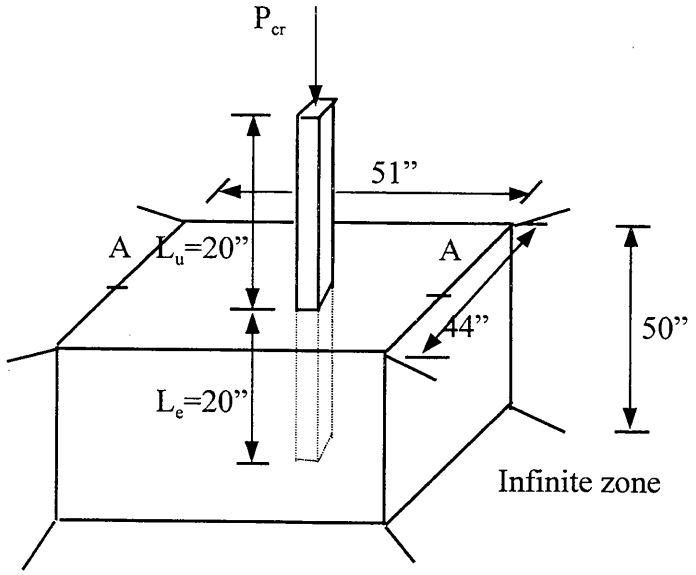

Fig. 4.5.2 Description of the single pile

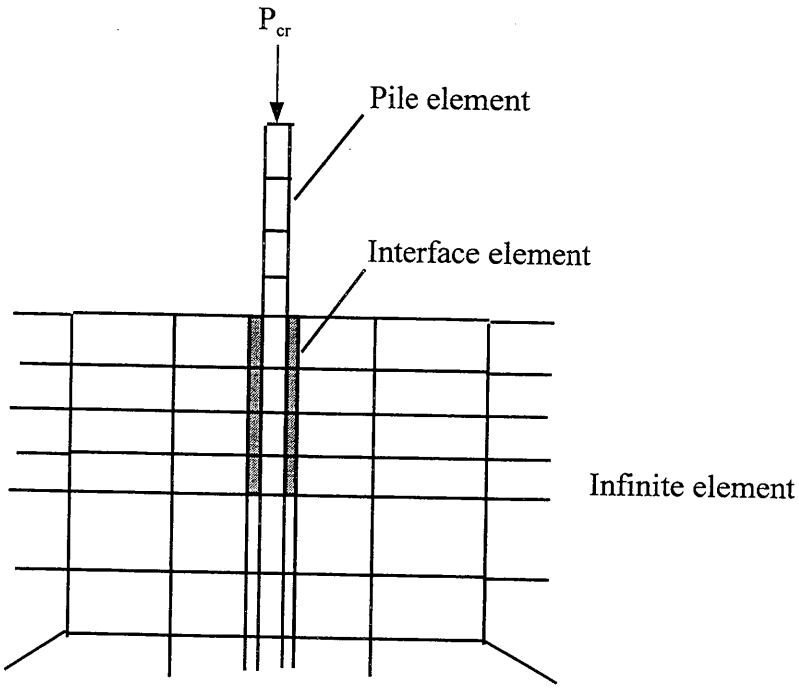

Fig. 4.5.3 Schematic diagram of finite element mesh for the section A-A of the single pile problem

4.5.2 Three-Pile Group

The description of the problem and the finite element mesh for the section A-A are given in Fig. 4.5.4 and 4.5.5. The buckling load for the three-pile group obtained using the present model is $P_{cr} = 288$ (lb) whereas the buckling load for a single-pile with free head is $P_{cr}=132$ (lb). Thus the buckling load for the three-pile group is less than the

sum of buckling loads of three individual free standing piles due to the interaction between the piles in the group.

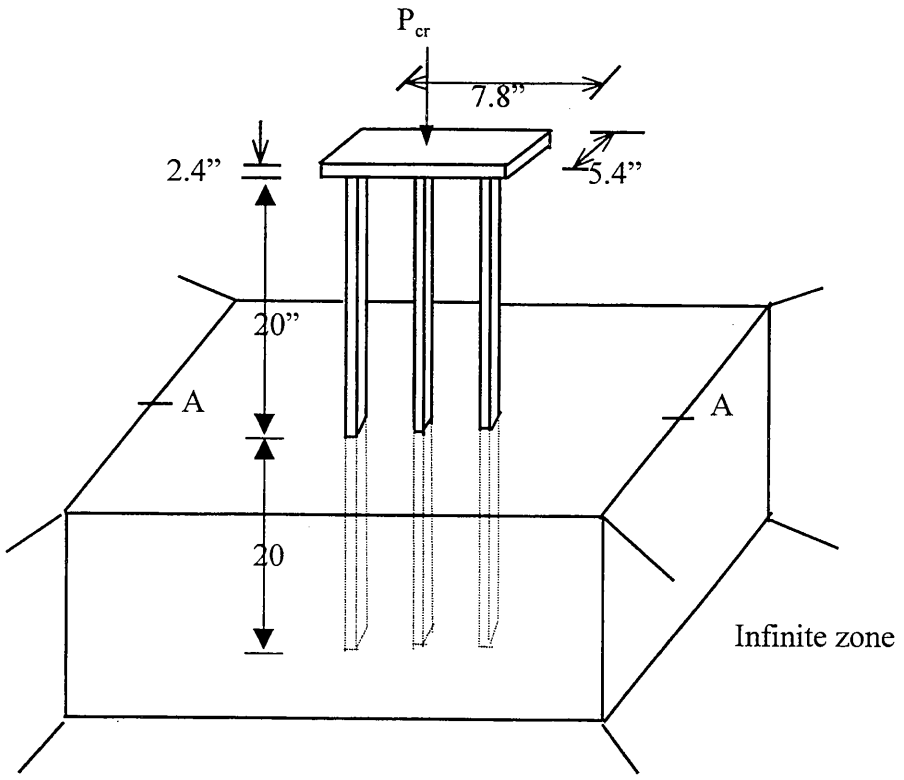

Fig. 4.5.4 Description of the three-pile group problem

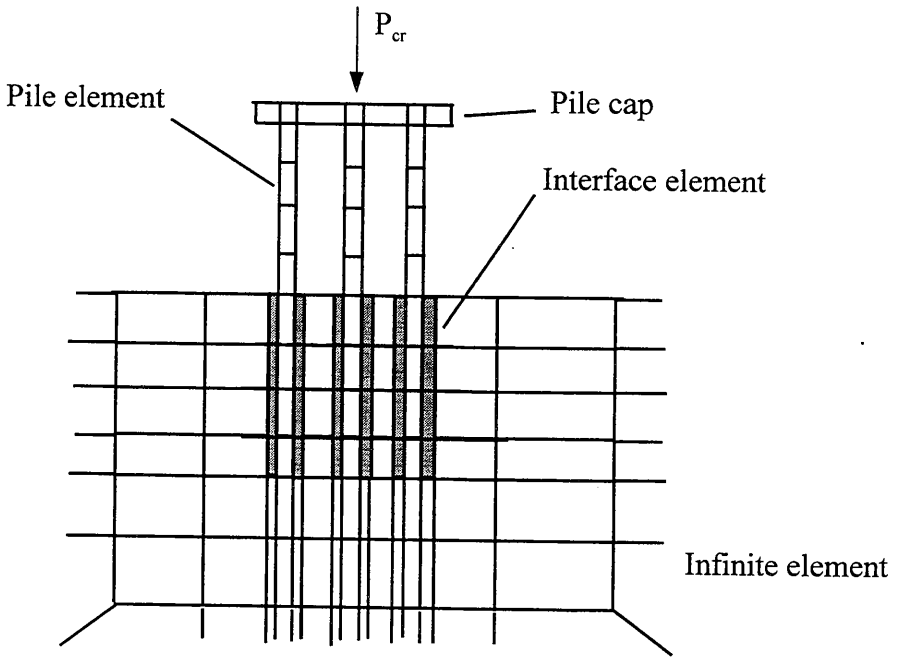

Fig. 4.5.5 Finite element mesh for the section A-A of the three-pile group problem

4.5.3 Six-Pile Group

For this problem shown in Fig. 4.5.6, 177 twenty-node elements and 3874 dof's were used. The finite element solution was obtained as P_{cr} = 2592 (lb) for the group of six piles with the length of unembedded part L_u =20 and the length of embedded part L_e =20. To see the effect of scouring, the problem with L_u=25 also was solved and the buckling load in this case is decreased to 1728 (lb) as expected.

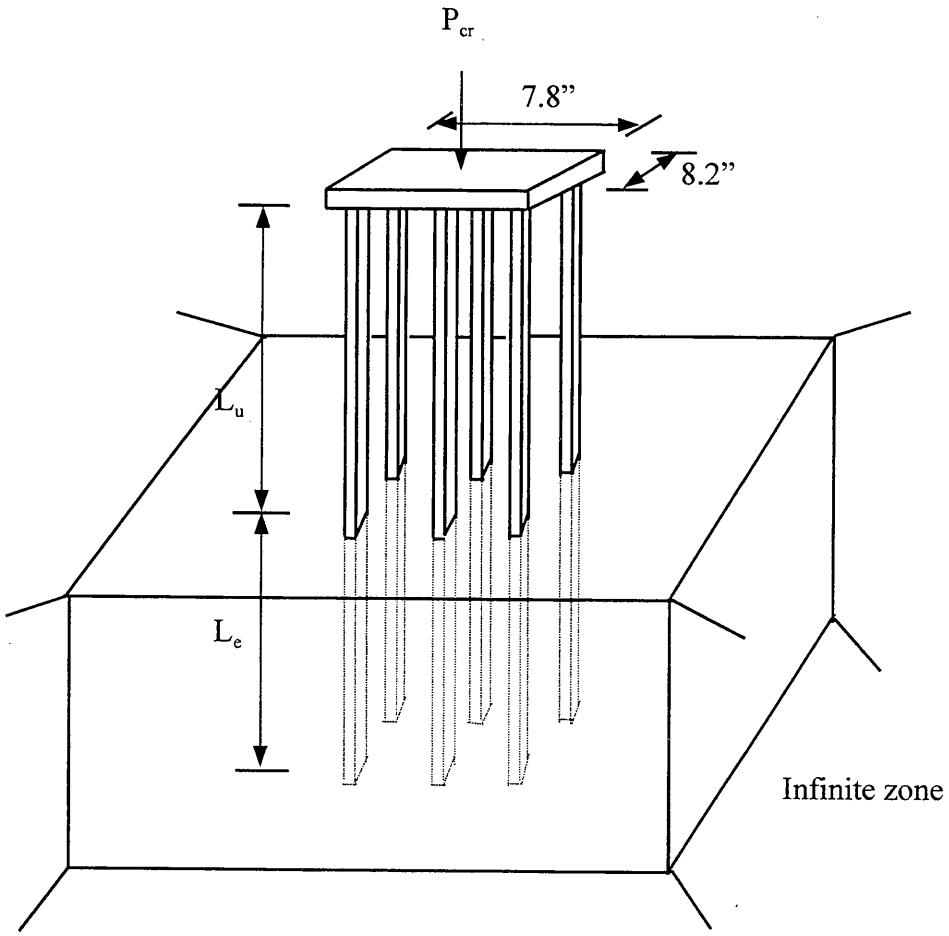

Fig. 4.5.6 Description of the six-pile group

To see how buckling load changes when non-vertical piles are used, the six-pile group shown in Fig. 4.5.7 was analyzed where the inclination angle of the non-vertical piles α is equal to 82.9°. The buckling load obtained is equal to 2616 (lb), which is little higher than that of the previous 6-pile group. This is because the non-vertical piles are in x-z plane whereas buckling occurs in y-z plane.

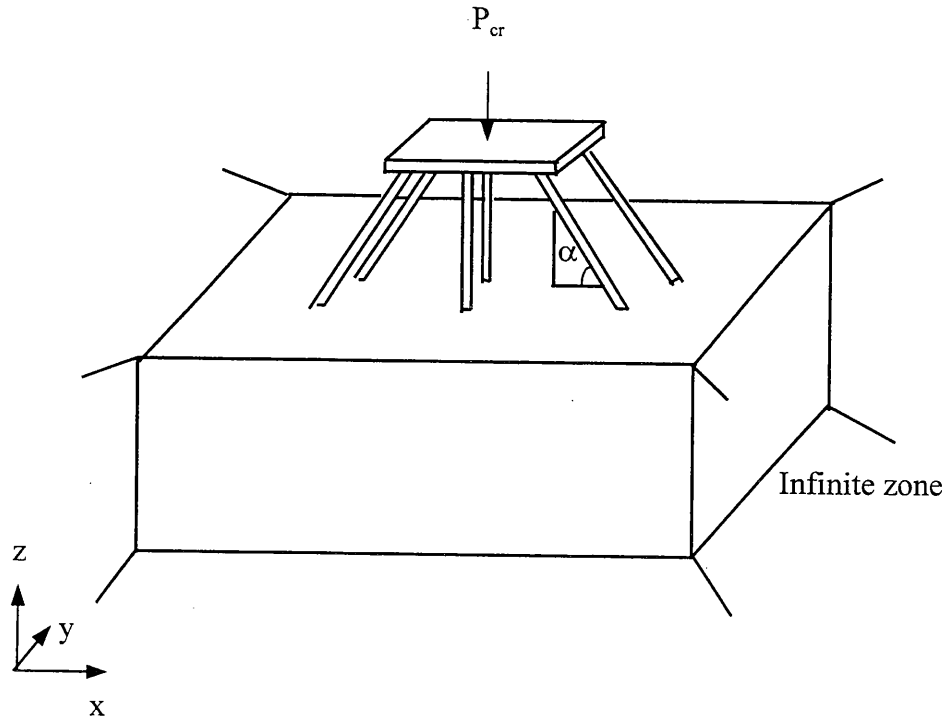

Fig. 4.5.7 Description of the six-pile group with non-vertical piles

Additional elastic support of the pile cap was considered in the finite element model to simulate the part of the bridge not present in the model. The spring has the stiffness $k_y=10^{10}$. For this value of the spring stiffness, it is found that the change in buckling load is negligibly small. However, this is likely to change if the stiffness of the spring reflects the properties of the structure more realistically.

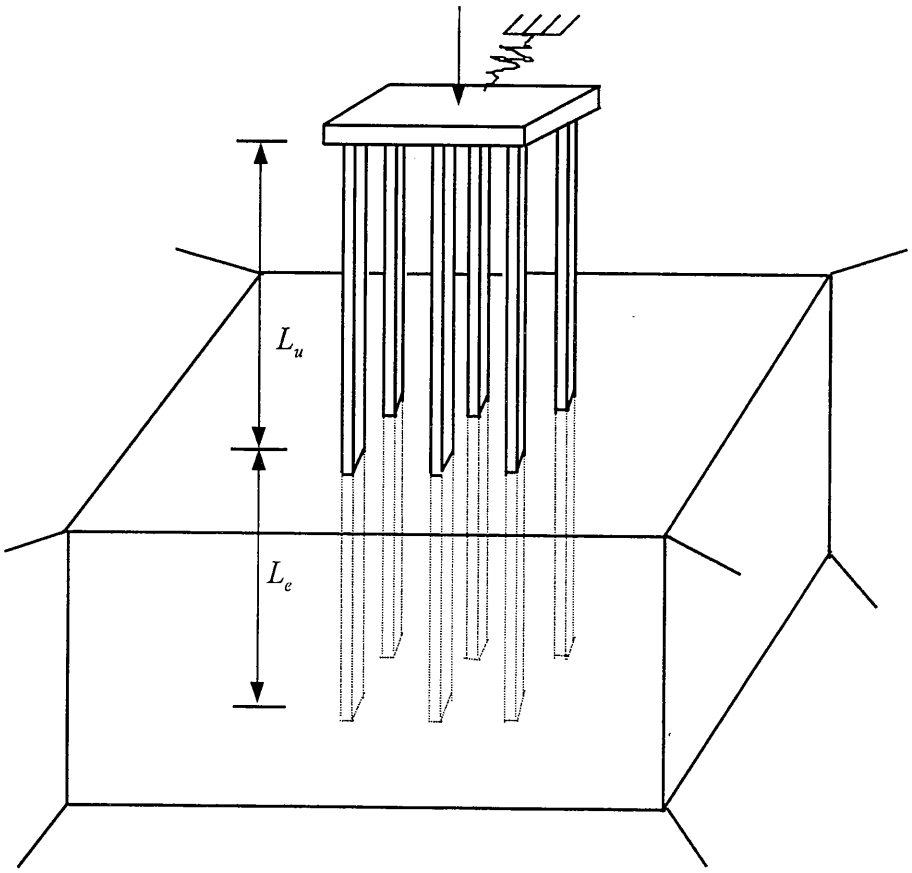

Fig. 4.5.8 Description of the six-pile group with an additional elastic support on the pile cap

CHAPTER 5
STRUCTURAL MODEL

For the continuum model developed in the previous chapter, the soil-pile interaction, pile-cap interaction and pile-soil-pile interaction are accounted for in an appropriate way. It is also capable to deal with any type of soil and pile groups. However, there is a problem with the continuum model. It is not feasible for a group with many piles due to the limitation of memory and disc space of the computer. So a new model needs to be developed for use in practice, which is called structural model. In this model, piles are modeled using beam-column elements undergoing large-deflection, and pile-soil interaction is modeled using nonlinear springs whose properties are expressed by p-y curves, t-z curves and end bearing curves. These curves are described in the existing literature (cited later in this report). Since it is difficult for the structural model to include precisely pile-soil-pile interaction for groups of closely spaced piles in which the spacing of the piles is less than six diameters, the continuum model is used together with the structural model to obtain the group-reduction factor to address the problem of pile interaction.

5.1 NONLINEAR FINITE ELEMENT FORMULATION FOR THIN-WALLED BEAMS

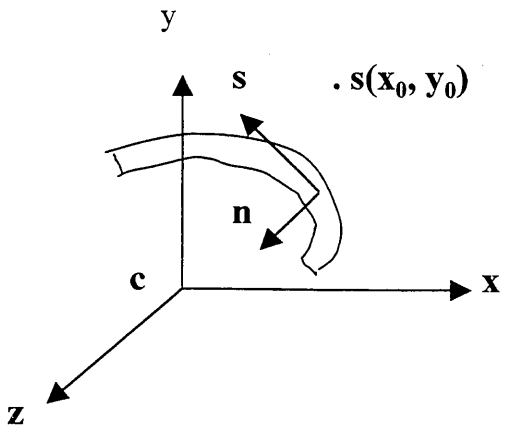

Fig. 5.1.1 Open, thin walled section

Fig. 5.1.1 represents a general open, thin-walled cross section. For small but finite deformation, the displacements of an arbitrary point on the cross section in the x, y and z directions may be expressed in terms of axial displacement of the centroid, the shear center displacements and the angle of rotation about the shear center axis,

$$U = u - (y - y_0)\Phi$$
$$V = v + (x - x_0)\Phi$$
$$W = w - x\,u_{,z} - y\,v_{,z} + (w_0 - \omega\,\Phi_{,z}) \qquad (5.1.1)$$

where x_0 and y_0 are the coordinates of the shear center, ω is the sectorial coordinate, u, v, w are displacements of the shear center while U, V, W are displacements of any point within the cross section.

In the present case, the components of the strain tensor are zero except the following

$$\varepsilon = W_{,z} + 0.5\,(U_{,z})^2 + 0.5\,(V_{,z})^2$$
$$\gamma_{zs} \approx 2n\,\Phi_{,z} \qquad (5.1.2)$$

where n is the normal distance from the shear center to a point of the cross section (Fig. 5.1.1).

Since the axial force due to warping is equal to zero, one has

$$\int_A E(w_{0,z} - \omega\Phi_{,zz})dA = EAw_{0,z} - E(\int_A \omega dA)\Phi_{,zz} = 0 \qquad (5.1.3)$$

or

$$w_{0,z} = (\frac{1}{A}\int_A \omega dA)\Phi_{,zz} \qquad (5.1.4)$$

Consequently, the following equations result from the Eq. 5.1.1

$$W_{,z} = w_{,z} - xu_{,zz} - yv_{,zz} + (\frac{1}{A}\int_A \omega\, dA - \omega)\Phi_{,zz}$$
$$= w_{,z} - xu_{,zz} - yv_{,zz} + \omega_n \Phi_{,zz}$$
$$U_{,z} = u_{,z} - (y - y_0)\Phi_{,z}$$
$$V_{,z} = v_{,z} + (x - x_0)\Phi_{,z} \qquad (5.1.5)$$

Thus, one has

$$\varepsilon = (w_{,z} - xu_{,zz} - yv_{,zz} + \varpi_n \Phi_{,zz}) + \frac{1}{2}[u_{,z} - (y - y_0)\Phi_{,z}]^2 + \frac{1}{2}[v_{,z} + (x - x_0)\Phi_{,z}]^2$$
$$\gamma = 2n\Phi_z \qquad (5.1.6)$$

Allowing only linear across thickness distribution of normal strain results in

$$\varepsilon = \varepsilon_0 + x\,\varepsilon_1 + y\,\varepsilon_2 + \varpi_n\,\varepsilon_\varpi \qquad (5.1.7)$$

where

$$\varepsilon_0 = w_{,z} + 0.5\,u_{,z}^2 + y_0\,u_{,z}\,\Phi_{,z} + 0.5\,y_0^2\,\Phi_{,z}^2 + 0.5\,v_{,z}^2 - x_0\,v_{,z}\,\Phi_{,z} + 0.5\,x_0^2\,\Phi_{,z}^2$$
$$\varepsilon_1 = -u_{,zz}^2 + v_{,z}\,\Phi_{,z} - x_0\,\Phi_{,z}^2$$
$$\varepsilon_2 = -v_{,zz}^2 - u_{,z}\,\Phi_{,z} - y_0\,\Phi_{,z}^2$$
$$\varepsilon_\omega = \Phi_{,z}^2 \qquad (5.1.8)$$

From the above expressions combined with the FE discretization, one can obtain

$$\begin{Bmatrix} \delta\varepsilon_0 \\ \delta\varepsilon_1 \\ \delta\varepsilon_2 \\ \delta\varepsilon_\omega \\ \delta\varepsilon_\gamma \end{Bmatrix} = \begin{Bmatrix} \underset{\sim}{B_0} \\ \underset{\sim}{B_1} \\ \underset{\sim}{B_2} \\ \underset{\sim}{B_\omega} \\ \underset{\sim}{B_\gamma} \end{Bmatrix} \delta \underset{\sim}{d} \qquad (5.1.9)$$

The use of the principle of virtual work leads to

$$\int_V (\sigma\delta\varepsilon + \tau\delta\gamma)dV = \int_L \int_A [\sigma(\delta\varepsilon_0 + x\delta\varepsilon_1 + y\delta\varepsilon_2 + \omega_n\delta\varepsilon_\omega + \tau(2n\delta\varepsilon_\gamma)]dAdz$$
$$= \delta \underset{\sim}{d}^T < \int_L \int_A [\sigma(\underset{\sim}{B_0^T} + x\,\underset{\sim}{B_1^T} + y\,\underset{\sim}{B_2^T} + \omega_n\,\underset{\sim}{B_\omega^T}) + \tau.2n.\,\underset{\sim}{B_\gamma^T}]dAdz$$
$$= \delta \underset{\sim}{d}^T < \int_L (N\underset{\sim}{B_0^T} - M_y\,\underset{\sim}{B_1^T} + M_x\,\underset{\sim}{B_2^T} + M_\omega\,\underset{\sim}{B_\omega^T}) + T_{SV}\,\underset{\sim}{B_\gamma^T}]dz$$
$$= 0 \qquad (5.1.10)$$

where

$$N = \int_A \sigma dA = \int_A E\varepsilon dA = EA\varepsilon_0$$
$$M_x = \int_A \sigma y dA = \int_A E\varepsilon y dA = EI_x \varepsilon_2$$
$$M_y = -\int_A \sigma x dA = -\int_A E\varepsilon x dA = -EI_y \varepsilon_1$$
$$M_\omega = \int_A \sigma\, \omega_n dA = \int_A E\varepsilon \omega_n dA = EI_\omega \varepsilon_\omega$$
$$T_{SV} = \int_A \tau.2ndA = \int_A G\gamma 2ndA = GJ\varepsilon_\gamma \qquad (5.1.11)$$

The above equations define the meaning of A, I_x, I_y, I_ω and J. Finally,

$$\underset{\sim}{f}^{\text{int}} = \int_L (N \underset{\sim}{B_0^T} - M_y \underset{\sim}{B_1^T} + M_x \underset{\sim}{B_2^T} + M_\omega \underset{\sim}{B_\omega^T} + T_{SV} \underset{\sim}{B_\gamma^T}) dz \qquad (5.1.12)$$

and the material part and geometrical part of the tangent stiffness matrix can be found to be

$$\underset{\sim}{K_m} = \int_L [\underset{\sim}{B_0^T}(EA)\underset{\sim}{B_0} + \underset{\sim}{B_1^T}(EI_y)\underset{\sim}{B_1} + \underset{\sim}{B_2^T}(EI_x)\underset{\sim}{B_2} + \underset{\sim}{B_\omega^T}(EI_\omega)\underset{\sim}{B_\omega} + \underset{\sim}{B_\gamma^T}(GJ)\underset{\sim}{B_\gamma}]dz$$
$$\underset{\sim}{K_g} = \int_L \underset{\sim}{H^T}(N \underset{\sim}{R_0} - M_y \underset{\sim}{R_1} + M_x \underset{\sim}{R_2}]\underset{\sim}{H}\, dz \qquad (5.1.13)$$

where

$$\underset{\sim}{R_0} = \begin{bmatrix} 0 & 0 & 0 & 0 & 0 & 0 & 0 \\ 0 & 1 & 0 & 0 & 0 & y_0 & 0 \\ 0 & 0 & 0 & 0 & 0 & 0 & 0 \\ 0 & 0 & 0 & 1 & 0 & -x_0 & 0 \\ 0 & 0 & 0 & 0 & 0 & 0 & 0 \\ 0 & y_0 & 0 & -x_0 & 0 & x_0^2 + y_0^2 & 0 \\ 0 & 0 & 0 & 0 & 0 & 0 & 0 \end{bmatrix} \qquad (5.1.14)$$

$$\underset{\sim}{R_1} = \begin{bmatrix} 0 & 0 & 0 & 0 & 0 & 0 & 0 \\ 0 & 1 & 0 & 0 & 0 & 0 & 0 \\ 0 & 0 & 0 & 0 & 0 & 0 & 0 \\ 0 & 0 & 0 & 0 & 0 & 1 & 0 \\ 0 & 0 & 0 & 0 & 0 & 0 & 0 \\ 0 & 0 & 0 & 1 & 0 & -2x_0 & 0 \\ 0 & 0 & 0 & 0 & 0 & 0 & 0 \end{bmatrix} \tag{5.1.15}$$

$$\underset{\sim}{R_2} = \begin{bmatrix} 0 & 0 & 0 & 0 & 0 & 0 & 0 \\ 0 & 1 & 0 & 0 & 0 & -1 & 0 \\ 0 & 0 & 0 & 0 & 0 & 0 & 0 \\ 0 & 0 & 0 & 1 & 0 & 0 & 0 \\ 0 & 0 & 0 & 0 & 0 & 0 & 0 \\ 0 & -1 & 0 & 0 & 0 & -2y_0 & 0 \\ 0 & 0 & 0 & 0 & 0 & 0 & 0 \end{bmatrix} \tag{5.1.16}$$

5.2 SOIL-PILE INTERACTION MODEL

In the structural model, nonlinear springs are used to model soil-pile interaction and p-y curves, t-z curves and end bearing curves are employed to express the properties of the springs. Typical curves for different types of soil and under different conditions are available in the references.

5.2.1 p-y Curves for Lateral Soil-Pile Interaction

p-y curve is the curve used to define the relationship between the lateral soil resistance p and the lateral pile deflection y. The two typical p-y curves are given in the following.

5.2.1a p-y curve for soft clay in the presence of free water

The procedure used to determine the p-y curve for short-term static loading of soft clay in the presence of free water is described in the following. The procedure resulted from experimental investigations [56].

1. Obtain the best possible estimate of the variation of undrained shear strength c and submerged unit weight γ with depth. Also obtain the value of ε_{50}, the strain corresponding to one-half of the maximum principal stress difference. Typical values of ε_{50} are as follows,

   ε_{50} = 0.02 for soft clay;
   0.01 for medium clay and
   0.005 for stiff clay. (5.2.1)

2. Compute the ultimate soil resistance per unit length of pile, using the smaller of the values given by the equation below.

$$P_u = [3+(\gamma'/c)x + (J/b)\ x\ ]cb \quad (5.2.2)$$

$$P_u = 9cb \quad (5.2.3)$$

where

γ' = average effective unit weight over the distance from ground surface to the location where p-y curve is to be determined,

x = depth from the ground surface to the location where p-y curve is to be found,

c = shear strength at depth x,

b = width of pile.

J = 0.5

3. Compute y_{50}, at one-half the maximum soil resistance from the following equation:

$$y_{50} = 2.5\ \varepsilon_{50} b \qquad (5.2.4)$$

4. Points describing the p-y curve at depth x are computed from the relationship:

$$p/p_u = 0.5(y/y_{50})^{1/3} \qquad (5.2.5)$$

The value of p remains constant beyond $y = 8y_{50}$.

5.2.1b p-y curve for sand above and below the water table

The procedure used to obtain the p-y curve for short-term static loading of sand above and below water table is described below. It follows the development reported in [56]

1. Obtain values for the angle of internal friction Φ, the soil unit weight γ, and pile diameter b.
2. Make the following preliminary computations:

$$\alpha = \Phi/2;\ \beta = 45 + \Phi/2;\ K_0 = 0.4;\ K_a = \tan^2(45 - \Phi/2), \qquad (5.2.6)$$

3. Compute the ultimate soil resistance per unit length of pile using the smaller of the values given by the following equations:

$$P_{st} = \gamma x [(K_0 x \tan \Phi \sin\beta) / (\tan(\beta - \Phi) \cos\alpha) + \tan\beta (b + x \tan\beta \tan\Phi) / \tan(\beta - \Phi) + K_0 x \tan\beta (\tan \Phi \sin\beta - \tan\alpha) - K_a b] \qquad (5.2.7)$$

$$P_{sd} = K_a b x \gamma[(\tan 8\beta)-1] + K_0 b \gamma x \tan \Phi \tan 4\beta \qquad (5.2.8)$$

4. In making the computation in step 3, find the depth x_t at which these two equations provide the same value. Above this depth use Eq. (5.2.7). Below this depth use Eq. (5.2.8).
5. Select a depth at which a p-y curve is desired.
6. Establish y_u as 3b/80. Compute p_u by the following equation:

$$p_u = A_s p_s \text{ or } p_u = A_c p_s. \qquad (5.2.9)$$

Use the appropriate value of A_s or A_c from Fig. 5.2.1 for the particular non-

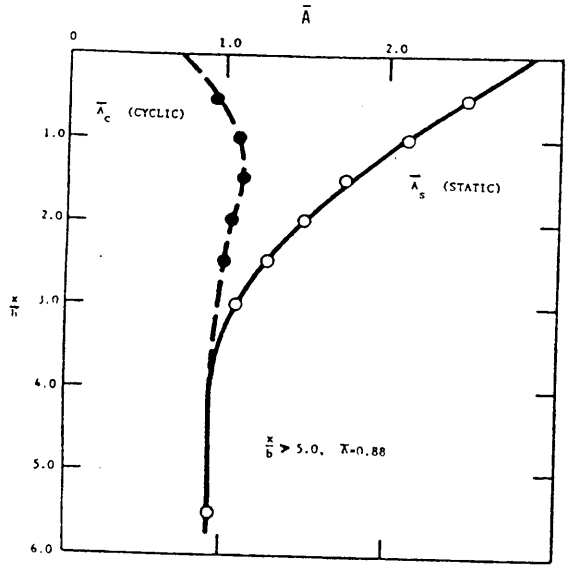

Fig. 5.2.1 Values of coefficients A_c and A_s

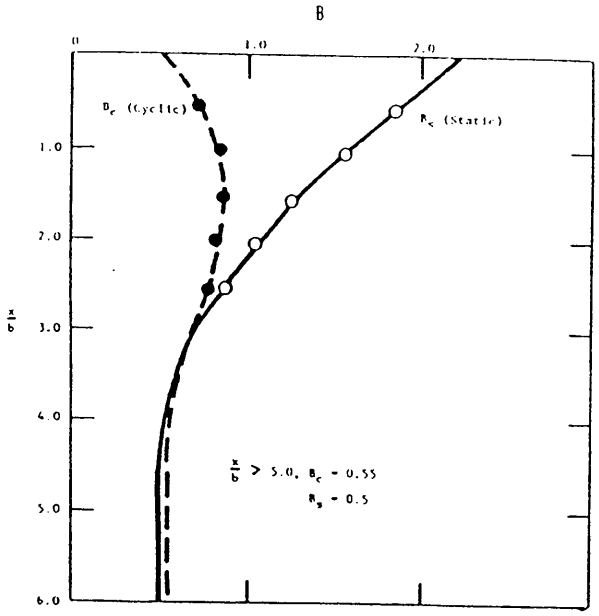

Fig. 5.2.2 Values of B for soil resistance versus depth

dimensional depth, and for the static or cyclic case. Use the appropriate equation for p_s, Eq. 5.2.7 or Eq. 5.2.8 by referring to the computation in Step 4.

7. Establish y_m as b/60. Compute p_m by the following equation:

$$p_m = B_s p_s \text{ or } p_m = B_c p_s. \quad (5.2.10)$$

Use the appropriate value of B_s or B_c from Fig. 5.2.2 for the particular non-dimensional depth, and for either the static or cyclic case. Use the appropriate equation for p_s. The two stright portions of the p-y curve, beyond the point where y is equal to b/60, can now be established.

8. Establish the initial straight-line portion of the p-y curve,

$$p = (k x) y \quad (5.2.11)$$

Use the appropriate value of k as follows:

For submerged sand

Relative density	Loose	Medium	Dense
Recommended k (lb/in^3)	20	60	125

For sand above water table

Relative density	Loose	Medium	Dense
Recommended k (lb/in^3)	25	90	225

9. Establish the parabolic section of the p-y curve,

$$p = Cy^{1/n} \quad (5.2.12)$$

Fit the parabola between points k and m as follows:

a. Get the slope of line between points m and u by

$$m = (p_u - p_m) / (y_u - y_m) \quad (5.2.13)$$

b. Obtain the power of the parabolic section by,

$$n = p_m / my_m \quad (5.2.14)$$

c. Obtain the coefficient C as follows:

$$C = p_m / y_m^{1/n} \tag{5.2.15}$$

d. Determine point k as,

$$y_k = (C / kx)^{n/n-1} \tag{5.2.16}$$

e. Compute appropriate number of points on the parabola by using Eq. 5.2.12.

5.2.2 t-z Curves for Vertical Soil-Pile Interaction

t-z curve is used to define the relationship between the shear load t on the surface of the pile and the pile shaft movement z. The typical t-z curves are for cohesive soil and cohesionless soil.

5.2.2a t-z Curve for Cohesive Soil

A t-z curve for cohesive soil is presented by the following table [56]

Table 5.2.1 Sample points for t-z curve for cohesive soil

Ratio of Load Transfer to Max. Load transfer	Pile Movement (in.)
0	0
0.18	0.01
0.38	0.02
0.79	0.04
0.97	0.06
1.00	0.08
0.97	0.12
0.93	0.16
0.93	0.20
0.93	>0.20

5.2.2b t-z Curve for Cohesionless soil [56]

A t-z curve for cohesionless soil is described by the use of the following equation:

$$f = \frac{w}{\frac{1}{E_s} + \frac{1}{f_{max}} w} \tag{5.2.17}$$

where

f = unit load transfer

w = pile movement

f_{max} = maximum unit load transfer

E_s = soil mudulus

5.2.3. End Bearing Curves

The end bearing curves are for predicting the load in end bearing of a pile as a function of the movement of the tip of the pile.

5.2.3a End Bearing Curve for Cohesive Soil

The equations describing the curve are as follows [56],

$$q_b = N_c (\sigma_f/2) \tag{5.2.18}$$

$$w_b = 2\varepsilon_{50} \tag{5.2.19}$$

where

q_b = failure stress in bearing at the base of footing.

σ_f = failure compressive stress in the laboratory unconfined compressive or quick triaxial test.

N_c = bearing capacity factor.

B = diameter of footing or eqivalent length of a side for a square or rectangular shape.

ε_{50} = strain measures from unconfined compression or quick triaxial test

w_b = settlement of footing or base of pile

5.2.3b End Bearing Curve for Cohesionless Soil

An equation for computing the load versus tip settlement for piles in sand is given as

$$q = (4z)^{1/3} q_{max} \tag{5.2.20}$$

where

z = tip settlement

q_{max} = maximum bearing capacity

$= \sigma_v N_q$

σ_v = the effective vertical stress which is equal to overburden pressure

$N_q = e^{\pi \tan\Phi} \tan^2(45+\Phi/2)$

5.3 GROUP EFFECT

The problem of closely-spaced piles in a group can be characterized as one of soil-pile interaction. A way to solve the problem is to introduce the p-factor and apply it to the p-y curves for a single pile, thus generating a new set of p-y curves that include the group effect. The p-factor is less than one and the magnitude depends on the configuration of piles in a group.

In the present study, both of these models were used to solve a number of identical problems to estimate the group factor. These factors should be used when structural model is employed. This would be the case in most practical situations since here the size of the problem prevents use of the continuum model. The result is shown in the following table.

Table 5.3.1 Group-reduction factor

p-factor	S/b
0.6	1
0.72	2
0.85	3
0.96	4
1.0	5

In the table, S is the center-to-center spacing of piles and b is the diameter of piles. A simple equation can be used for obtaining the p-factor:

$$p-factor=\begin{cases}0.5+0.1*(S/b) & 1\le S/b\le 5\\ 1.0 & S/b\ge 5\end{cases}$$

5.4 RESULTS AND DISCUSSIONS RELATED TO STRUCTURAL MODEL

A computer program named MN_PILE_GROUP for stability analysis of three-dimensional pile groups has been developed based on the structural model presented in this chapter. The program has the capacity to deal with the plastic hinge formation and elastic support at the cap level. The problems in this chapter were solved using MN_PILE_GROUP.

5.4.1 Verification

Several examples were designed to verify agreement of the results obtained in this study with the existing available analytical solutions. They were also designed to address some comments voiced during our meeting with Mn/DOT personnel. The following particular cases were considered.

Case 1

For a fully embedded simply supported pile (HP12x53) with lateral soil-pile interaction modeled by constant spring stiffness K_p, analytical solution is available and given by Timoshenko [57]. Our finite element solution is very close to Timoshenko's solution and shown in Fig. 5.4.1.

Case 2

To see how side friction affects buckling load, a fully embedded pile (HP12x53) supported by a roller located at the top, elastic support at the bottom, and by side friction

modeled as axial spring of stiffness K_t is considered and the results are given in Fig. 5.4.2. It can be seen that side friction makes buckling load higher. The reason for this is that side friction affects load transfer mechanism and the axial force in the pile decreases with the depth due to this effect. Therefore the upper part of the pile plays a dominant role in the process of buckling. This is somewhat equivalent to reducing the effective length of the pile.

Case 3

In this case, buckling of a single pile for various value of both side friction and lateral soil resistance is considered. A fully embedded simply supported pile (HP12x53) is solved for different values of K_t and K_p, and the result is shown in Fig. 5.4. 3, where K_{p0} and K_{t0} represent the initial values of K_p and K_t. As expected, buckling load is increased with the increase of K_{p0} and K_{t0}.

Case 4

A fully embedded pile (HP12x53) without side friction is considered to see the effect of the stiffness K_b of the end bearing on buckling load. The result is shown in Fig. 5.4.4. It turns out that the buckling load is independent of K_b when side friction is absent, which is in agreement with both analysis and intuition.

Case 5

To show how buckling load varies with the stiffness K_p for lateral soil resistance when side friction is present a fully embedded pile (HP12x53) is solved and the result is plotted in Fig. 5.4.5. It can be seen that buckling load increases faster with increasing K_p when K_p is small. These calculations have been conducted in response to some comments from the Mn/DOT personnel indicating that small lateral resistance significantly changes the buckling load. The results obtained here show that this is indeed the case if comparison is made with buckling load corresponding to no lateral support ($K_p = 0$).

However, even for larger values of K_p, the buckling load increases with increasing K_p (as it should).

Case 6

This final example is solved to see how buckling load varies with pile length for different values of stiffness K_p for lateral soil resistance. The pile is fully embedded supported by a roller at the top, end bearing at the bottom and, lateral support K_p. The results in Figs. 5.4.6 – 5.4.11 show that buckling load decreases quickly with pile length when the value of K_p is smaller and buckling load changes little when pile length goes beyond a certain value, especially for bigger K_p. In all cases, an asymptotic value of the buckling load seems to be approached which is in agreement with expectations voiced by the Mn/DOT personnel during the meeting. However, for very large values of K_p the buckling load exhibits a different variation – at some point it increases with the length. This is in agreement with other results reported in literature.

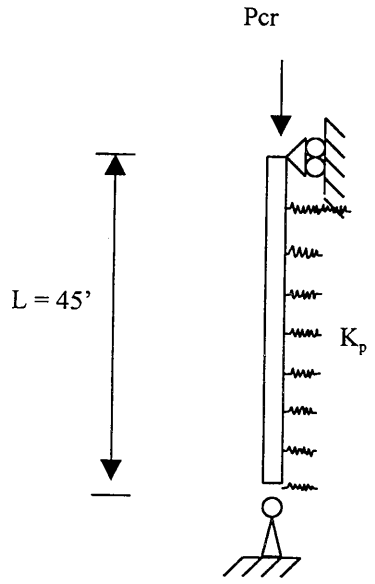
Pcr
L = 45'
K_p

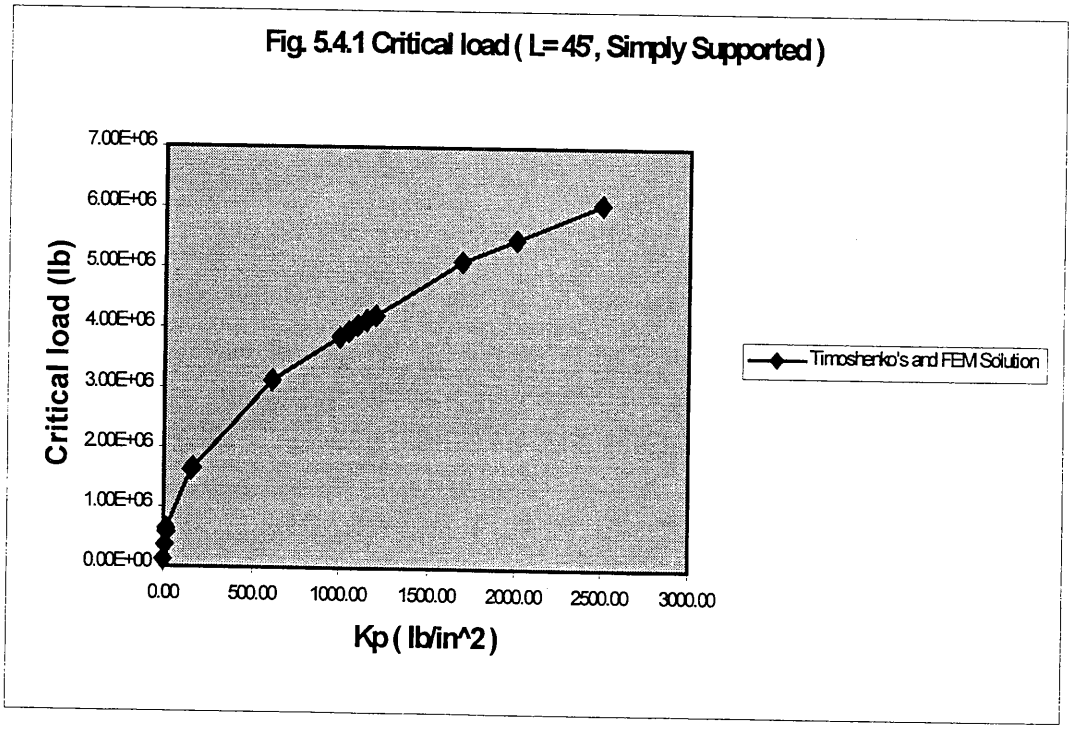
Fig. 5.4.1 Critical load (L= 45', Simply Supported)
Critical load (lb)
7.00E+06
6.00E+06
5.00E+06
4.00E+06
3.00E+06
2.00E+06
1.00E+06
0.00E+00
0.00
500.00
1000.00
1500.00
2000.00
2500.00
3000.00
Kp (lb/in^2)
Timoshenko's and FEM Solution

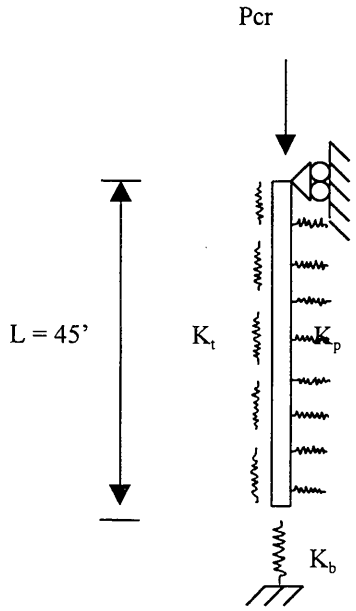
Pcr
L = 45'
K_t
K_p
K_b

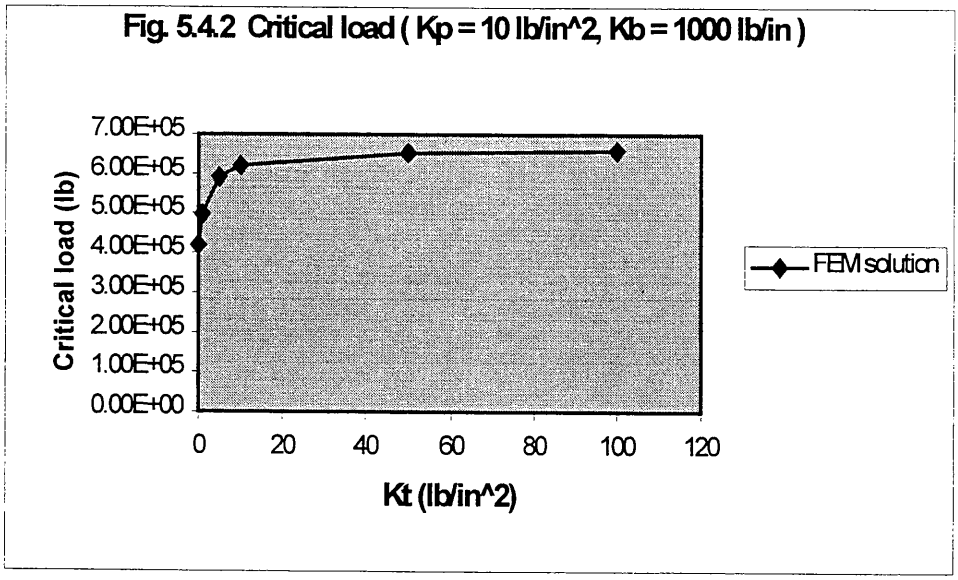
Fig. 5.4.2 Critical load (Kp = 10 lb/in^2, Kb = 1000 lb/in)
Critical load (lb)
7.00E+05
6.00E+05
5.00E+05
4.00E+05
3.00E+05
2.00E+05
1.00E+05
0.00E+00
0
20
40
60
80
100
120
Kt (lb/in^2)
FEM solution

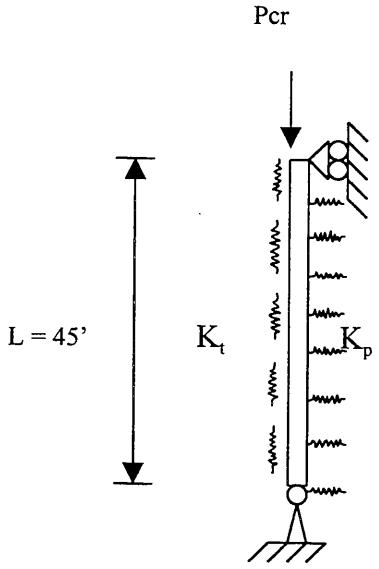
Pcr
L = 45'
K_t
K_p

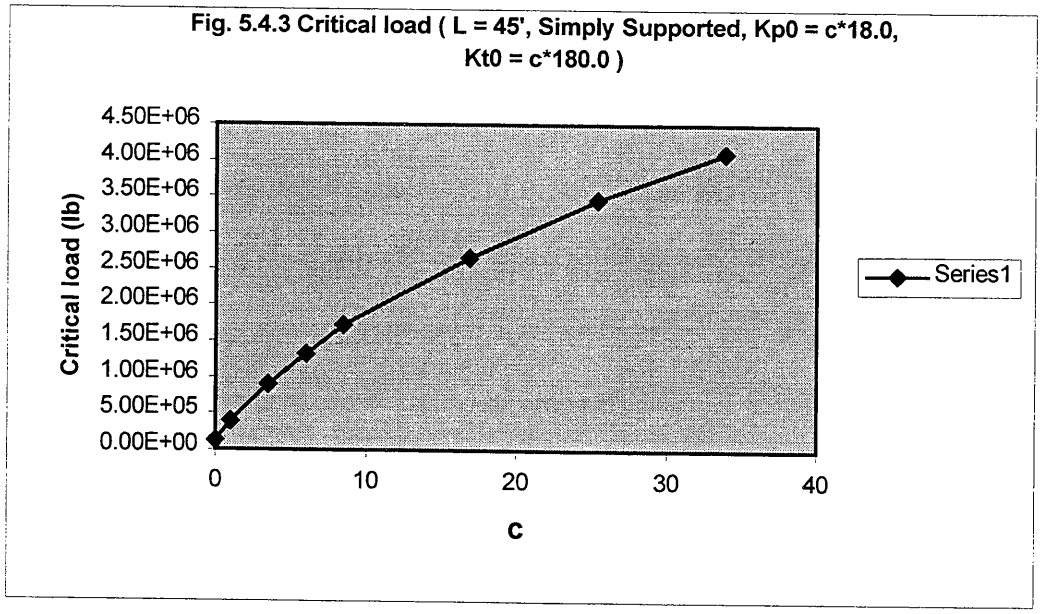
Fig. 5.4.3 Critical load (L = 45', Simply Supported, Kp0 = c*18.0, Kt0 = c*180.0)
Critical load (lb)
4.50E+06
4.00E+06
3.50E+06
3.00E+06
2.50E+06
2.00E+06
1.50E+06
1.00E+06
5.00E+05
0.00E+00
0
10
20
30
40
c
Series1

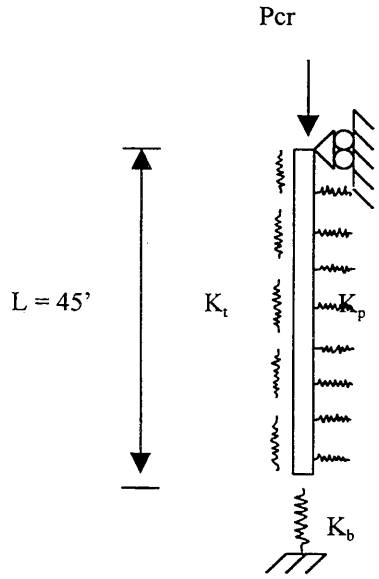
Pcr
L = 45'
K_t
K_p
K_b

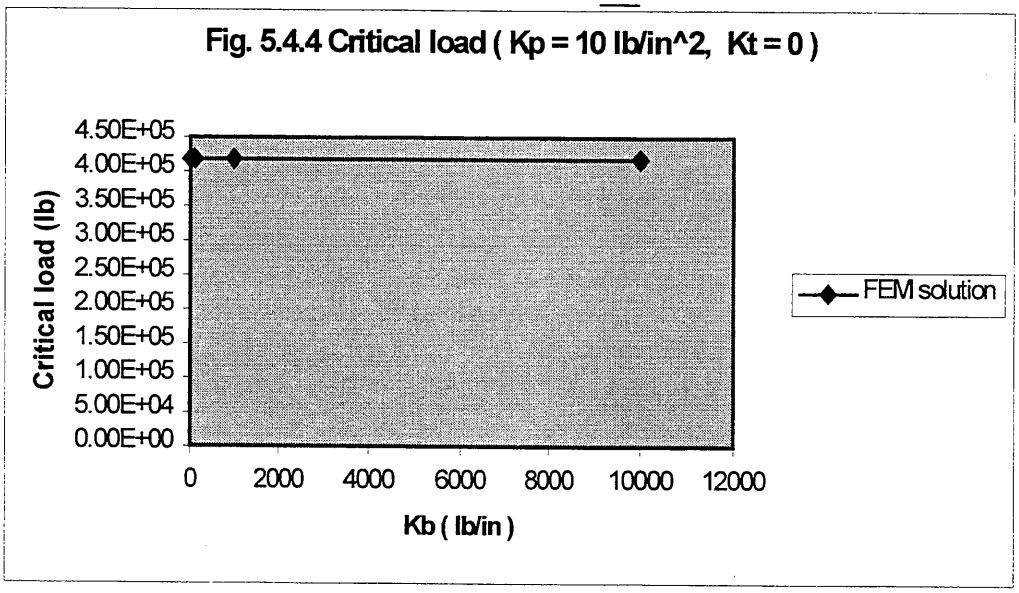
Fig. 5.4.4 Critical load (Kp = 10 lb/in^2, Kt = 0)
Critical load (lb)
4.50E+05
4.00E+05
3.50E+05
3.00E+05
2.50E+05
2.00E+05
1.50E+05
1.00E+05
5.00E+04
0.00E+00
0
2000
4000
6000
8000
10000
12000
Kb (lb/in)
FEM solution

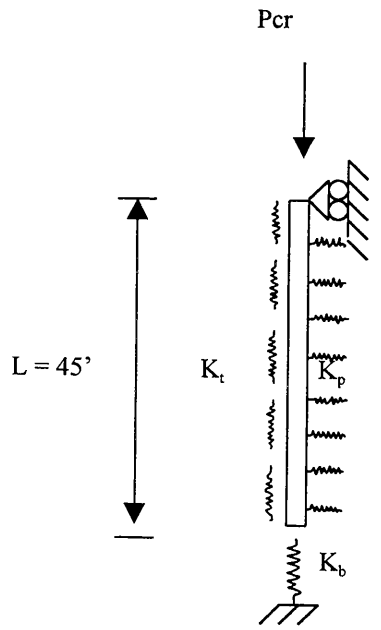
Pcr
L = 45'
K_t
K_p
K_b

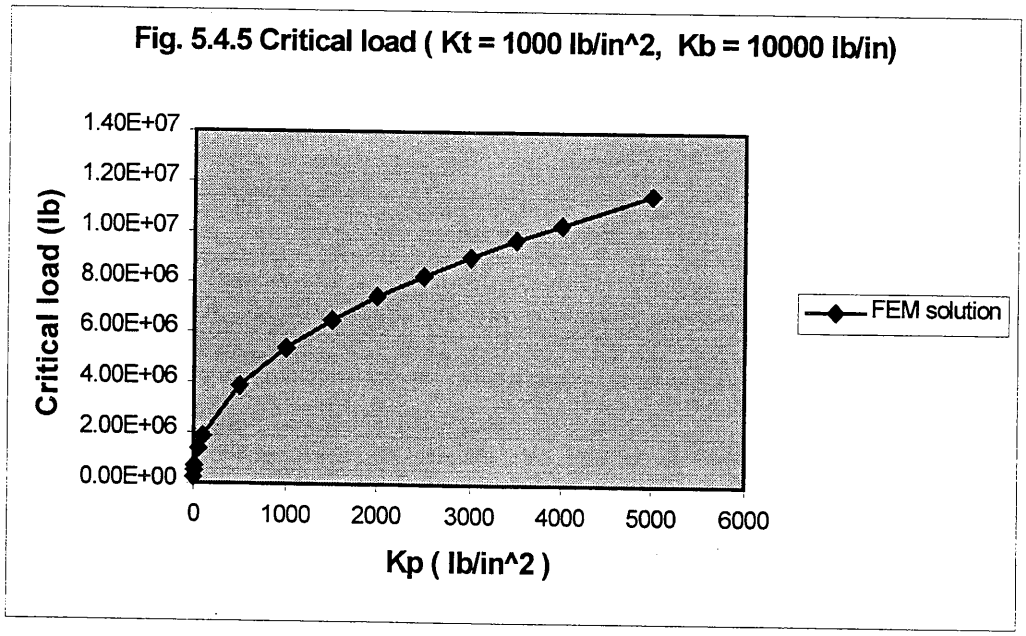
Fig. 5.4.5 Critical load (Kt = 1000 lb/in^2, Kb = 10000 lb/in)
Critical load (lb)
1.40E+07
1.20E+07
1.00E+07
8.00E+06
6.00E+06
4.00E+06
2.00E+06
0.00E+00
0
1000
2000
3000
4000
5000
6000
Kp (lb/in^2)
FEM solution

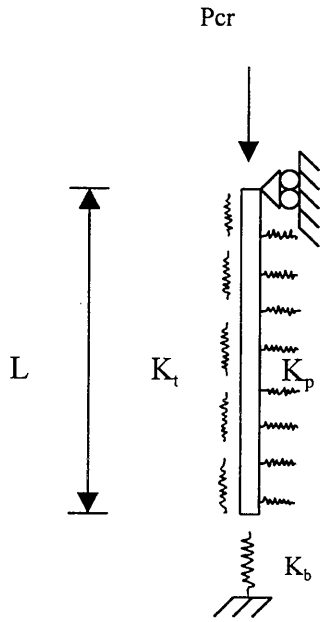
Pcr
L
K_t
K_p
K_b

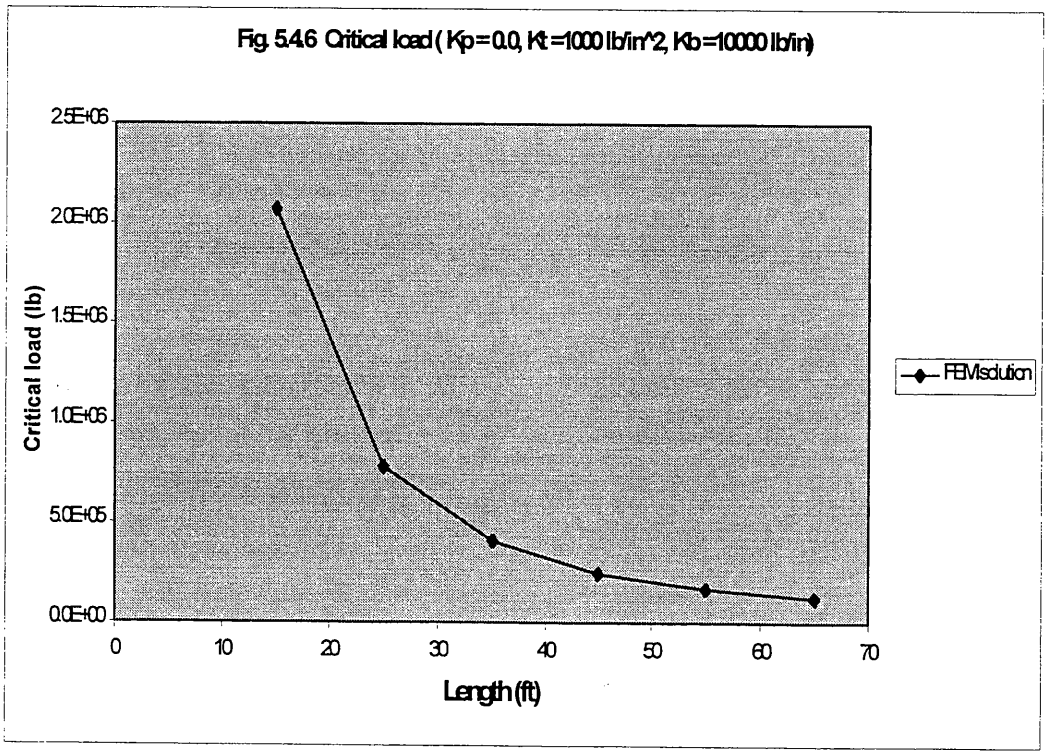
Fig. 5.4.6 Critical load (Kp=0.0, Kt=1000 lb/in^2, Kb=10000 lb/in)
Critical load (lb)
2.5E+06
2.0E+06
1.5E+06
1.0E+06
5.0E+05
0.0E+00
0
10
20
30
40
50
60
70
Length (ft)
FEMsolution

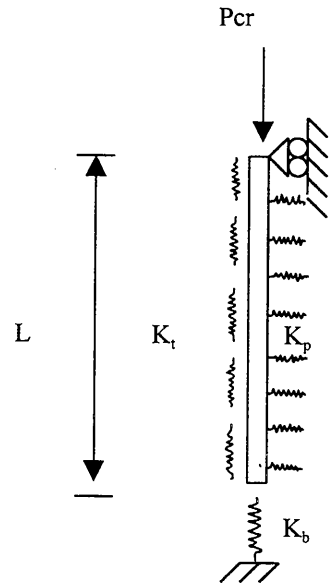
Pcr
L
K_t
K_p
K_b

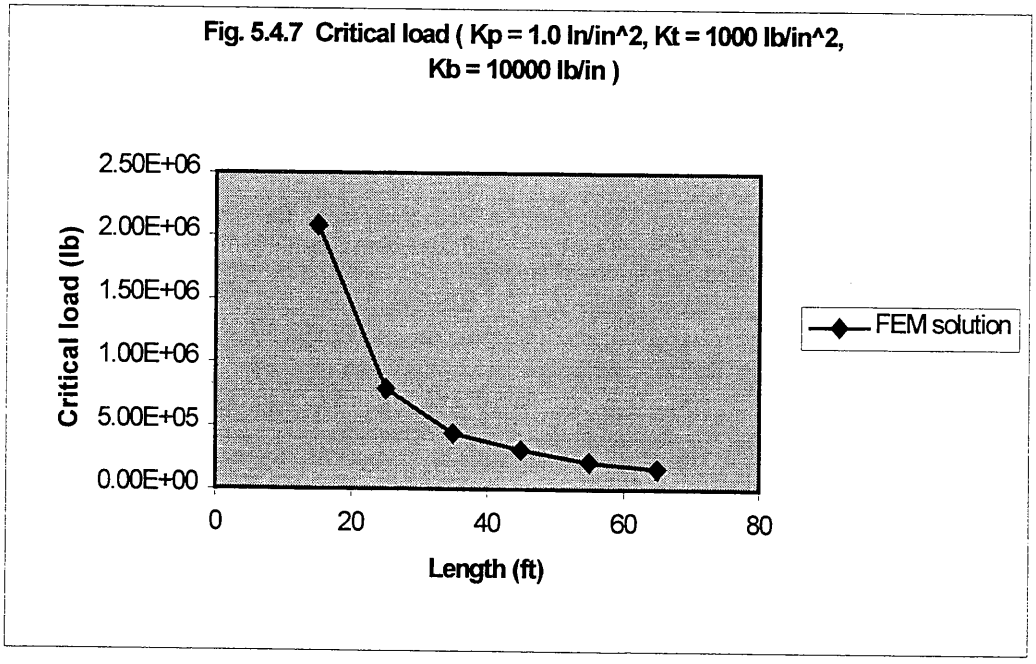
Fig. 5.4.7 Critical load (Kp = 1.0 lb/in^2, Kt = 1000 lb/in^2, Kb = 10000 lb/in)
2.50E+06
2.00E+06
1.50E+06
1.00E+06
5.00E+05
0.00E+00
Critical load (lb)
0
20
40
60
80
Length (ft)
FEM solution

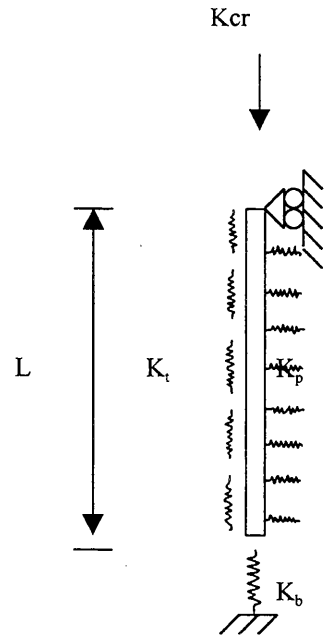
Kcr
L
K_t
K_p
K_b

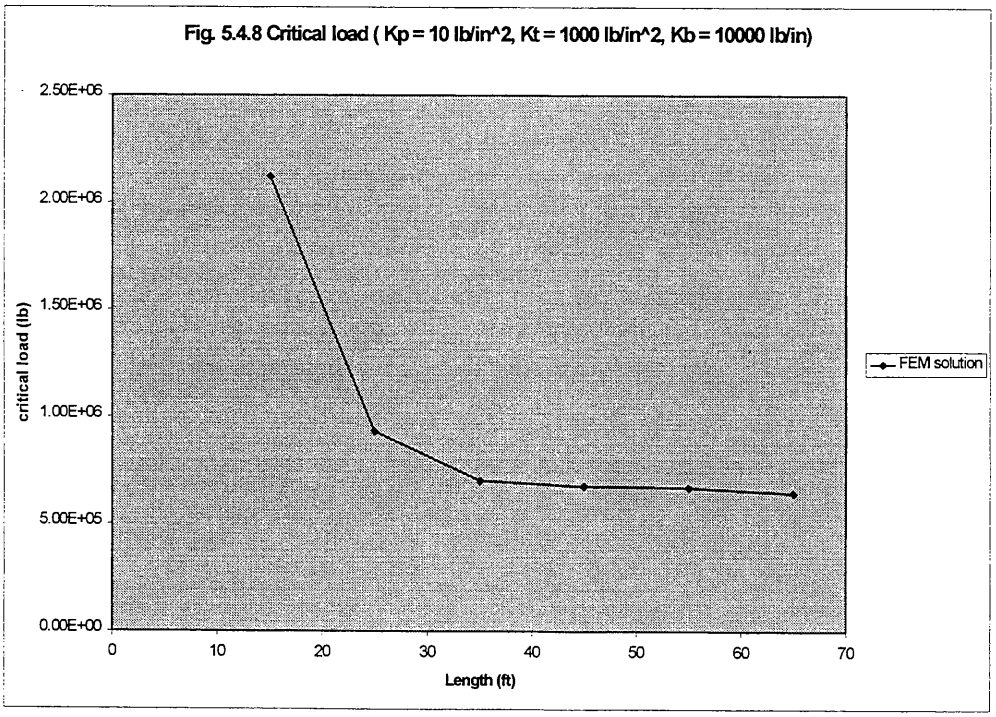
Fig. 5.4.8 Critical load (Kp = 10 lb/in^2, Kt = 1000 lb/in^2, Kb = 10000 lb/in)
2.50E+06
2.00E+06
1.50E+06
1.00E+06
5.00E+05
0.00E+00
critical load (lb)
0
10
20
30
40
50
60
70
Length (ft)
FEM solution

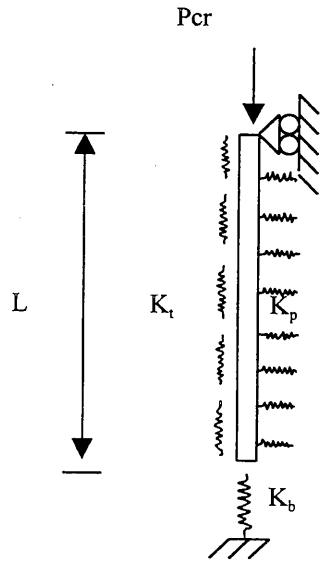
Pcr
L
K_t
K_p
K_b

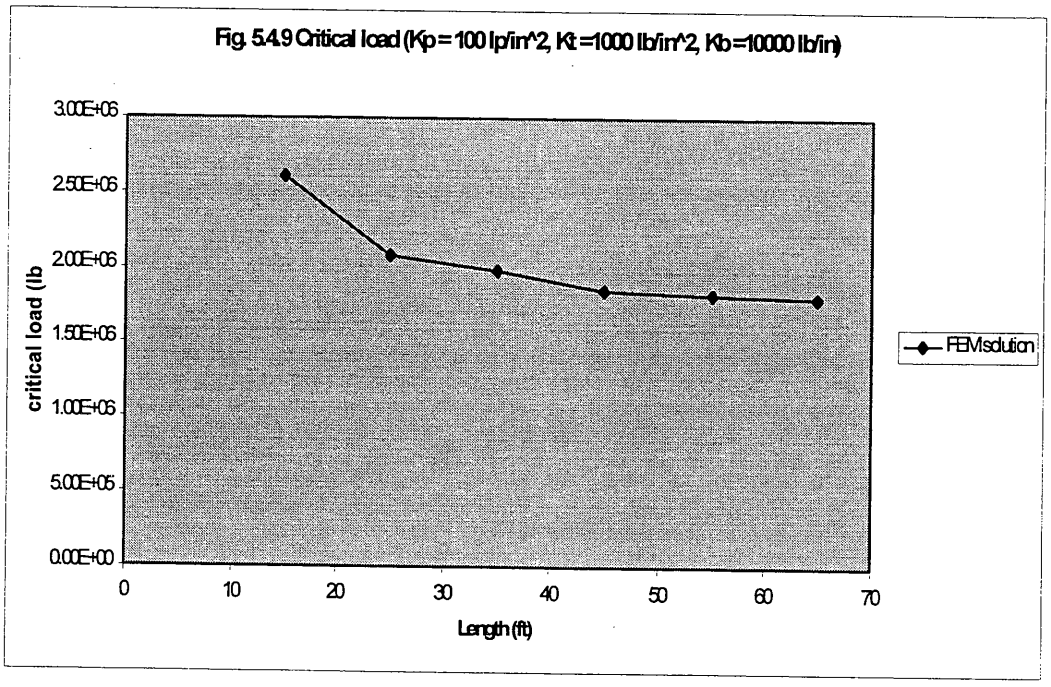
Fig. 5.4.9 Critical load (Kp = 100 lp/in^2, Kt =1000 lb/in^2, Kb =10000 lb/in)
3.00E+06
2.50E+06
2.00E+06
1.50E+06
1.00E+06
5.00E+05
0.00E+00
critical load (lb
0
10
20
30
40
50
60
70
Length (ft)
FEM solution

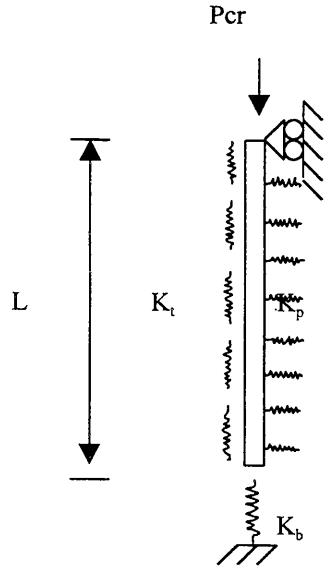
Pcr
L
K_t
K_p
K_b

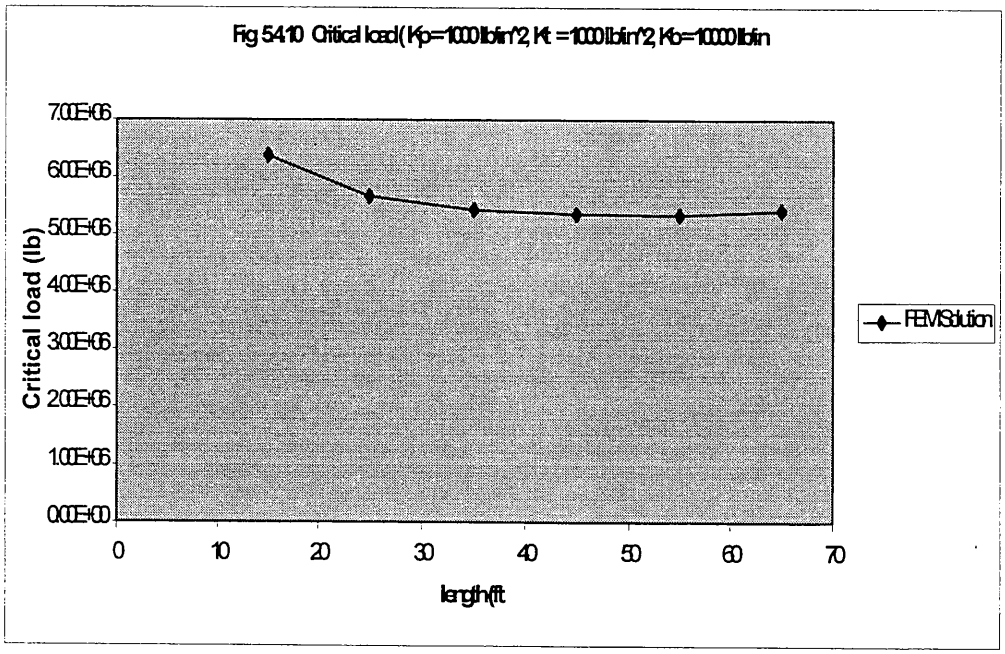
Fig 5.4.10 Critical load (Kp=1000 lb/in^2, Kt =1000 lb/in^2, Kb=10000 lb/in
Critical load (lb)
7.00E+06
6.00E+06
5.00E+06
4.00E+06
3.00E+06
2.00E+06
1.00E+06
0.00E+00
0
10
20
30
40
50
60
70
length(ft
FEMSolution

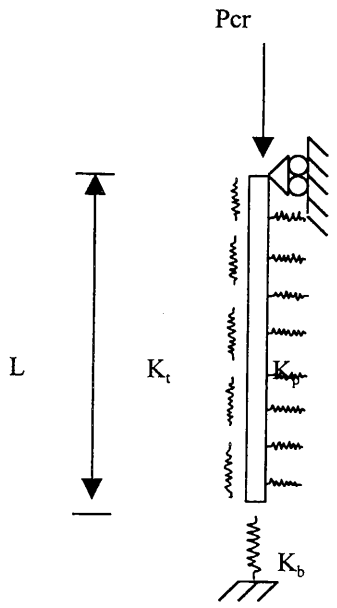
Pcr
L
K_t
K_p
K_b

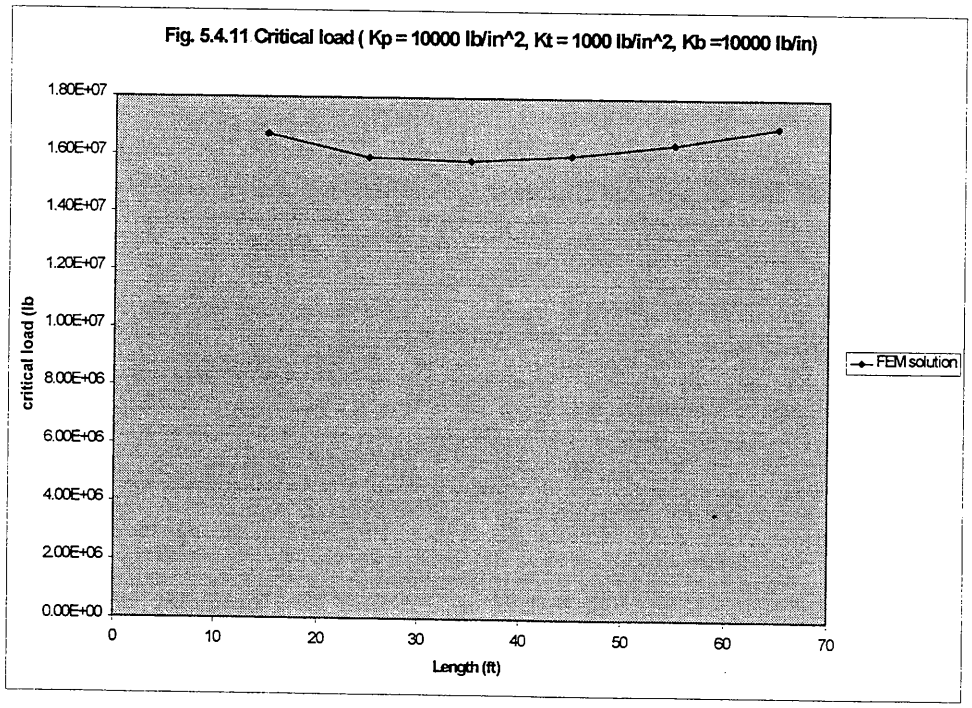
Fig. 5.4.11 Critical load (Kp = 10000 lb/in^2, Kt = 1000 lb/in^2, Kb =10000 lb/in)
1.80E+07
1.60E+07
1.40E+07
1.20E+07
1.00E+07
8.00E+06
6.00E+06
4.00E+06
2.00E+06
0.00E+00
critical load (lb
0
10
20
30
40
50
60
70
Length (ft)
FEM solution

5.4.2. Effect of Various Parameters

The effect of important parameters on buckling loads is illustrated through the following examples, in which an embedded CIP concrete pile with the diameter of 16 inches and the length of 540 inches is considered and modeled using ten elements. The elastic modulus of the pile is 3640 ksi.

5.4.2a For p-y curve

Consider soft clay in the presence of free water. Two values of the shear strength of soil are taken and the result is shown here:

Shear strength c =500 (lb/ft^2) : P_{cr} = 480.5 (kips)

Shear strength c =800 (lb/ft^2) : P_{cr} = 532.6 (kips)

5.4.2b For t-z Curve

(a) Cohesionless soil

Maximum load transfer f_{max} = 2095.0 (lb/ft): P_{cr} = 648.5 (kips)

Maximum load transfer f_{max} = 2509.0 (lb/ft): P_{cr} = 789.2 (kips)

(b) Sand below the water table

Angle of internal friction $\Phi = 30^0$: P_{cr} = 648.5 (kips)

Angle of internal friction $\Phi = 35^0$: P_{cr} = 714.2 (kips)

5.4.2c For end bearing curve

Consider conhesionless soil. The effect of variation of angle of internal friction is shown in the following:

Angle of internal friction $\Phi = 30^0$: P_{cr} = 789.2 (kips)

Angle of internal friction $\Phi = 35^0$: P_{cr} = 726.1 (kips)

5.4.3 Comparison of the Continuum model and Structural Model

A six-pile group described in section 4.5.3 is analyzed using the continuum and structural model, respectively. The result is as follows:

(a) Continuum model

$L_u = 20$ (in): $P_{cr} = 2592$ (lb)

$L_u = 25$ (in): $P_{cr} = 1728$ (lb)

(b) Structural model (no pile-soil-pile interaction considered)

$L_u = 20$ (in): $P_{cr} = 2914$ (lb)

$L_u = 25$ (in): $P_{cr} = 2035$ (lb)

(c) Structural model (Group-reduction p-factor = 0.7 used)

$L_u = 20$ (in): $P_{cr} = 2650$ (lb)

$L_u = 25$ (in): $P_{cr} = 1763$ (lb)

It can be seen that for the continuum model one has

$$6*P_{single} > P_{group} \quad (P_{single}=495 \text{ lb for } L_u=20 \text{ in.})$$

whereas for the structural model without the use of p-factor

$$6*P_{single} \cong P_{group} \quad (P_{single}=481 \text{ lb for } L_u=20 \text{ in.})$$

The reason for this is that group effect is included in the continuum model. When the structural model is used in combination with the group-reduction p-factor, the result is very close to that obtained using the continuum model, which is expected.

5.4.4 Results for the Three Pile-Groups

Data for the bridge piers described in this section was provided by Mn/DOT. Drawings describing these bridges are quite involved and provided data used here. These drawings should be consulted for details; here only scheches of the piers are given to describe the problem schematically. The piers were analyzed using structural model described in Chapter 5.

(a) Bridge # 08003

The description of a group of 24 HP12x53 piles with length 45 (ft) is given in Fig. 5.4.12. The elastic modulus of the piles is 29,000 ksi, and the cohesion and shear strength of the soil are taken as 830 (psf) and 500 (lb/ft^2), respectively. The pile cap is

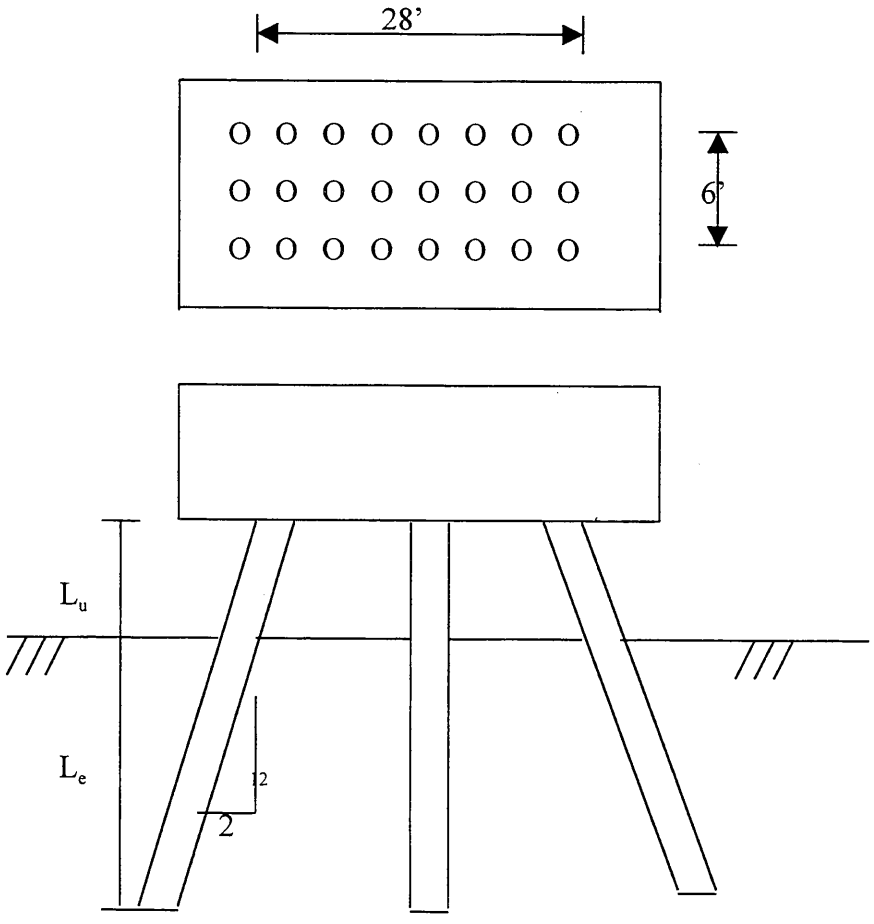

Fig. 5.4.12 Description of a pile-group for the bridge # 08003

set free to move and a single concentrated load applied at the center of the cap is considered to cause buckling. The result is shown in Table 5.4.1.

Table 5.4.1 Critical load of a pile-group for the bridge # 08003

	Critical load
L_u = 10 (ft), L_e = 35 (ft)	8216 (kips)
L_u = 14 (ft), L_e = 31 (ft)	6704 (kips)
L_u = 20 (ft), L_e = 25 (ft)	4518 (kips)
L_u = 30 (ft), L_e = 15 (ft)	2630 (kips)

(b) Bridge # 80004

Fig. 5.4.13 shows a pile-group composed of 8 CIP concrete 16'' piles with the cap free to move. The elastic modulus of the piles is 3,640 ksi, the soil cohesion is 4500 psf and shear strength is 2000 lb/ft^2. The result is given in Table 5.4.2.

Table 5.4.2 Critical load of a pile-group for the bridge # 80004

	Critical load
L = 45 (ft), L_u = 0	3960 (kips)
L = 45 (ft), L_u = 20 (ft)	2570 (kips)
L = 45 (ft), L_u = 30 (ft)	1250 (kips)
L = 55 (ft), L_u = 0	3610 (kips)
L = 55 (ft), L_u = 20 (ft)	2440 (kips)
L = 55 (ft), L_u = 30 (ft)	1130 (kips)

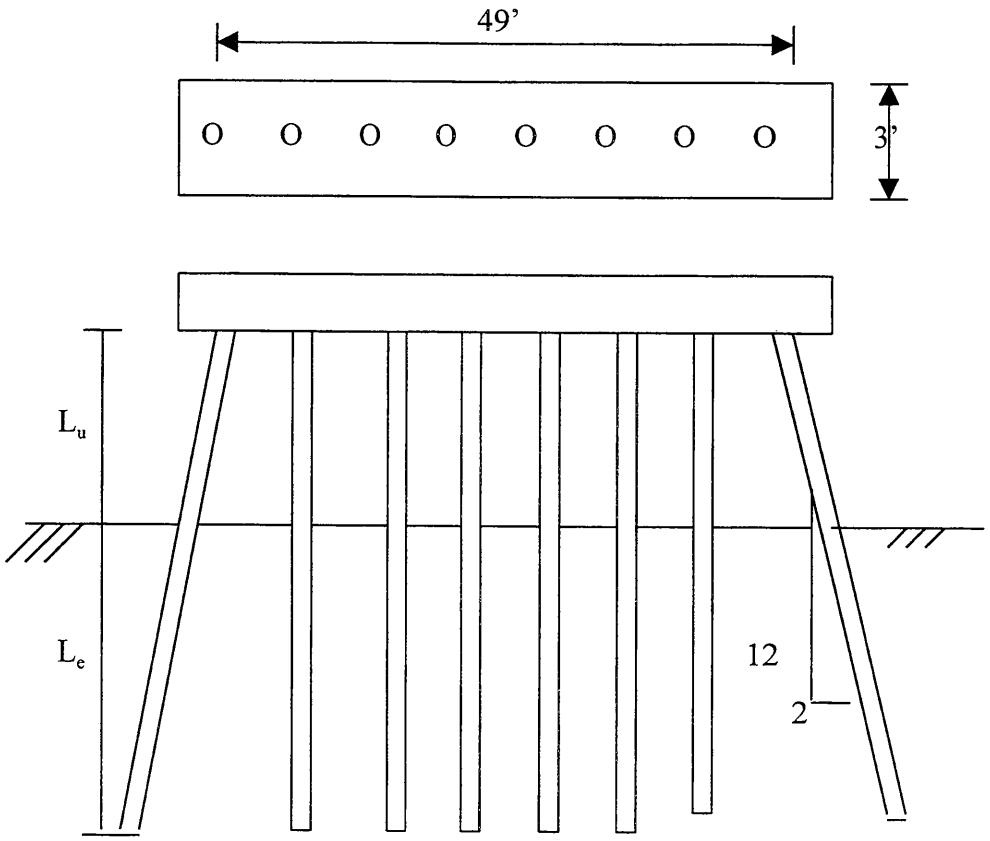

Fig. 5.4.13 Description of a pile-group for the bridge # 80004

(c) Bridge # 5930

Fig. 5.4.14 shows a pile-group for the bridge # 5930, in which 16 CIP concrete 16'' piles are used. The elastic modulus of the pile is 3,640 ksi and the pile length is 72 ft. The value of internal friction angle of the soil is taken as 35^0. The result is ahown in Table 5.4.3.

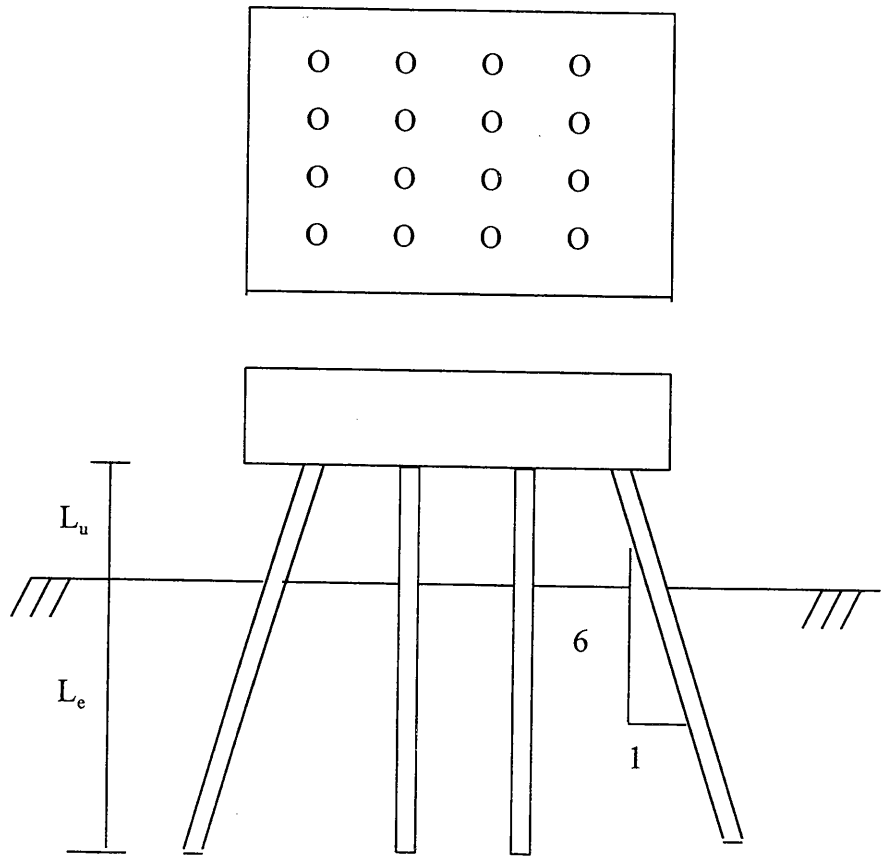

Fig. 5.4.14 Description of a pile-group for the bridge # 5930

Table 5.4.3 Critical load of a pile-group for the bridge # 5930

	Critical load
Lu = 0	4980 (kips)
L_u = 10 (ft)	4740 (kips)
L_u = 30 (ft)	2610 (kips)

CHAPTER 6
CLOSURE

A continuum model and a structural model are proposed and implemented for stability of pile groups in the present study. The continuum model accounts for pile-soil interaction, pile-cap interaction and pile-soil-pile interaction in an appropriate way. It is also capable to deal with any type of soil and pile groups (layered soil, battered piles, etc.). However, the continuum model is not feasible for practical use because of the limitation of memory and disc space of the computer. In contrast, the structural model is efficient and simple to implement, but it is difficult to include pile-soil-pile interaction. Both of these models were used to solve a number of identical problems to estimate the group factor. These factors, which depend on the configuration of the pile group, should be used when structural model is employed. This would be the case in most practical situations since here the size of the problem prevents use of the continuum model.

The structural model has been incorporated in the computer program MN_PILE_GROUP. Since it can run efficiently on a personal computer, it is easily accessible to all bridge engineers for analysis related to design or maintenance purpose.

It needs to be remembered that the accuracy of the predicted buckling load depends on the adequate description of the problem, particularly on accurate description of the properties of the soil. The program MN_PILE_GROUP includes soil models found in the literature, which are considered to be appropriate for most common types of the soil. At the same time this part of the model is perhaps one that is the most difficult to quantify and is likely to be the most significant source of the errors in the predicted buckling load. In this context, the benefits of having a computer code MN_PILE_GROUP can only be realized by considering a range of the soil properties that can possibly characterize specific site and computation of the corresponding range of buckling loads. This would require several runs of the program (for several possible data representing a given site), but efficiency of MN_PILE_GROUP should easily allow for

that. The resulting range of buckling loads should then give a good conservative value of the buckling load.

REFERENCES

1. Adachi, T., and Kimuram M.,"Model test and analysis of interaction factor on laterally loaded group piles", Num. Models Geomech., Pande, G.N. (ed), Balkema, 1992, pp.309-318.
2. Bergan, P.G., Horrigmoe, G., Krakeland, B., and Soreide, T.H.,"Solution techniques f or nonlinear finite element problems", Int. J. Num. Meth. Eng., Vol.12 (1978), pp.1677-1696.
3. Bettess, P. and Zienkiewicz, O.C.,"Diffraction and refraction of surface waves using finite and infinite elements", Int. J. Num. Meth. Eng., Vol.11 (1977), pp.1271-1290.
4. Bhowmik, S.K.,"3-D nonlinear finite element analysis of laterally loaded piles in clay", Ph.D. Thesis, Univ. of Illinois, Urbana, 1992.
5. Brandtzaeg, A. and Harboe, E.,"Buckling tests of slender steel piles in soft, quick clay", Proc. 4th. Int. Conf. Soil Mech. Found. Eng., 1957, pp.19-23.
6. Brebbia, C.A. and Walker, S., Boundary Element Techniques in Engineering, Newnes-Butterworth, London, 1980.
7 . Budkowska, B.B. and Szymczak, C.,"Partially embedded piles subjected to critical buckling load-sensitivity analysis", Comput. Struct., Vol. 61 (1996), pp.193-196.
8 . Budkowska,B.B. and Czymczak, C.,"Initial post-buckling behavior of piles partially embedded in soil", Comput. Struct., Vol.62 (1997), pp.831-835.
9 . Chen, L.T. and Poulos, H.G.,"Piles subjected to lateral soil movements", J. Geotech. Environmental Eng., Vol.123 (1997), pp.802-811.
10 Chow, Y.K.,"Analysis of piles used for slope stabilization", Int. J. Num. Anal. Geomech., Vol.20 (1996), pp.635-646.
11. Crisfield, M.A.,"A fast incremental/iterative solution procedure that handles snap-through", Compt. Struct., Vol.13 (1981), pp.55-62.
12. Davisson, M.T. and Robinson, K.E., "Bending and buckling of partially embedded piles", Proc. 6th Int. Conf. Soil Mech. Found. Eng., Montreal, Canada, Vol 2 (1965), pp.243-246.
13 Day,R.A. and Potts, D.M.,"Zero thickness interface elements-numerical stability

and application", Int. J. Num. Anal. Meth. Geomech., Vol.18 (1994), pp.689-708.

14. Desai, C.S., Zaman, M.M., Lightner, J.G. and Siriwardane, H.J., "Thin-layer element for interfaces and joints", Int. J. Num. Anal. Meth. Geomechanics, Vol 8 (1984), pp.19-43.
15. DiMaggio, F.L and Sandler, I.S.,"Material model for granular soils", J. Eng. Mech. Div., ASCE, Vol.97, No.3, (1971).
16. Dou, H., and Byrne, P.M.,"Dynamic response of single piles and soil-pile interaction", Canadian Geotech. J., Vol.33 (1996), pp.80-96.
17. Emson, C., and Bettess, P.,"Application of infinite elements to external electromagnetic field problems", Proc. Int. Conf. Num. Meth. Coupled Problems, E. Hinton et al (eds), Pineridge Press, 1981, pp.887-902.
18. Frank, R., Guenot, A. and Humbert, P.,"Numerical analysis of contacts in geomechanics", Proc. 4th. Int. Conf. Num. Meth. Geomech., Rotterdam, 1982, pp.37 -42.
19. Gabr, M.A. and Wang, J.,"Buckling of friction piles supporting bridge foundations", Transp. Res. Rec. 1447, Transportation Research Board, Washington, D.C., pp.93 -101.
20. Gabr, M.A., Wang, J.J. and Zhao,M.,"Buckling of piles with general power distribution of lateral subgrade reaction", J. Geotech. Environmental Eng., Vol.123 (1997), pp.123-130.
21. Ghaboussi, J., Wilson, E.L. and Isenberg, J.," Finite element for rock joint interfaces", J. Soil Mech. Foundations Div., ASCE, Vol.99 (1973), pp.833-848.
22. Golder, H.G., and Skipp, B.O.,"The buckling of piles in soft clay", Proc. 4th Int. Conf. Soil Mech. Found. Eng., 1957, pp.35-39.
23. Goodman, R.E., Taylor, R.L. and Brekke, T.L.,"A model for the mechanics of jointed rock", J. Soil Mech. Foundations Div., ASCE, Vol.94 (1968), pp.637-659.
24. Griffiths, D.V.,"Numerical modeling of interfaces using conventional finite elements", Proc. 5th Int. Conf. Num. Meth. Geomech., Nagoya, 1985,, pp.837-844.
25. Hermann, L.R.,"Finite element analysis of contact problems", Proc. ASCE, Vol.104 (1978), pp.1043-1057.

26. Hoit, M.I., McVay, M. and Andrade, P.W., "Nonlinear pile foundation analysis using Florida-pier", J. Bridge Eng., Vol.1 (1996), pp.135-142.
27. Hohberg, J.M. and Schweiger, H.F.,"On the penalty behavior of thin-layer elements", Num. Models Geomech., Pande and Pietruszczak (eds), 1992, Balkema, pp.241-248.
28. Katona, M.G.,"A simple friction-contact interface element with applications to buried culverts", Int. J. Num. Anal. Meth. Geomech., Vol.7 (1983), pp.371-384.
29. Kaynia, A.M., and Mahzooni, S.,"Forces in pile foundations under seismic loading", J. Eng. Mech., Vol.122 (1996), pp.46-53.
30. Keller, H.B.,"Numerical solution of bifurcation and nonlinear eigenvalue problems", Applications of Bifurcation Theory, P.H. Rabinowitz (ed), Academic Press, New York, 1977, pp.359-384.
31. Langen, H.V., et al,"Interface elements for singular plasticity points", Int. J. Num. Anal. Meth. Geomech., Vol.15 (1991), pp.301-315.
32. Lay, J.Y., et al,"A residual-force FE approach to soil-structure interaction analysis", Int. J. Num. Anal. Meth. Geomech., Vol.15 (1991), pp.181-203.
33. Li, H. and Saigal, S., "Mapped infinite element for 3-D vector potential magnetic problems", Int. J. Num. Meth. Eng., Vol 37 (1994), pp.343-356.
34. Muqtadir, A. and Desai, C.S.,"Three-dimensional analysis of a pile-group foundation", Int. J. Anal. Meth. Geomech., Vol.10 (1986), pp.41-58.
35. Pande, G.N. and Sharma, K.G.,"On joint/interface elements and associated problems of numerical ill-conditioning", Int. J. Num. Anal. Meth. Geomech., Vol.3 (1979), pp.293-300.
36. Poskitt, T.J., "The deflection of piles during driving", Geotechniques, Vol.46 (1996), pp.235-243.
37. Ramm, E.,"Strategies for tracing the nonlinear response near limit points", Nonlinear Finite Element Analysis in Structural Mechanics, W.Wunderlich, E. Stein and K.J.Bathe (eds), Springer, 1981, pp.63-89.
38. Reddy, A.S. and Valsangkar, A.J., "Buckling of fully and partially embedded piles", J. Soil Mech. Found. Div., ASCE, Vol 96, No SM6 (1970), pp.1951-1965.
39. Reese, S. and Wriggers, P., "A finite element method for stability problems in

finite elasticity", Int. J. Num. Meth. Eng., Vol.38 (1995), pp1171-1200.

40. Riks, E.,"An incremental approach to the solution of snapping and buckling problems", Int. J. Solids Struct., Vol.15 (1979), pp.529-551.
41. Roscoe, K.H. and Burland, J.B.,"On the generalized stress-strain behavior of wet clays", Engineering Plasticity, Herman, F. and Leckie, F.A. (eds), Cambridge University Press, 1968.
42. Sachdeva, T.D. and Ramakrishnan, " A finite element solution for the two dimensional elastic contact problem", Int. J. Num. Meth. Eng., Vol.17 (1981), pp.1257-1271.
43. Schweizerhof, K.H. and Wriggers, P.,"Consistent linearization for path following methods in nonlinear FE analysis", Comput. Meth, Appl. Mech. Eng., Vol.59 (1986), pp.261-279.
44. Selby, A.R. and Arta, M.R.,"Three-dimensional finite element analysis of pile groups under lateral loading", Comput. Struct., Vol.40 (1991), pp.1329-1336.
45. Shi, J.,"Computing critical points and secondary paths in nonlinear structural stability analysis by the finite element method", Comput. struct., Vol.58 (1996), pp.203-220.
46. Siriwardane, H.J. and Desai, C.S.,"Computational procedures for nonlinear three-dimensional analysis with some advanced constitutive laws", Int. J. Num. Anal. Meth. Geomech., Vol.7 (1983), pp.143-171.
47. Spence, A., and Jepson, A.D.,"The numerical calculation of cusps, bifurcation points and isola formation points in two parameter problems", Numerical Methods for Bifurcation Problems, ISNM 70, 1984, pp.502-514.
48. Trochanis, A., Bielak, J. and Christiano, P., "Three-dimensional nonlinear study of piles", J. Geotech. Eng., Vol.117 (1991), pp.429-447.
49. Wagner, W, and Wriggers, P.,"A simple method for the calculation of postcritical branches", Eng. Comput., Vol.5 (1988), pp.103-109.
50. Wriggers, P., Wagner, W. and Miehe, C., "A quadratically convergent procedure for the calculation of stability points in finite element analysis", Compt. Meth. Appl. Mech. Eng., Vol 70 (1988), pp. 329-347.

51. Wriggers, P and Simo, J.C., " A general procedure for the direct computation of turning and bifurcation points", Int. J. Num. Meth. Eng., Vol 30 (1990), pp.155-176.
52. Zaman, A.M. and Desai, C.S., "Interface model for dynamic soil-structural interaction", J. Geotechnical Eng., Vol 110 (1984), pp.1257-1273.
53. Zaman, M.M., et al,"Effects of cap thickness and pile inclination on the response of a pile group foundation by a 3-D FE analysis", Compt. Geotechnics, Vol.15 (1993), pp.65-86.
54. Zienkiewicz. O.C., Kelly, D.W. and Bettess, P.,"The coupling of the finite element and boundary solution procedures", Int.J.Num.Meth.Eng., Vol.11 (1977), pp.355-375.
55. Zienkiewicz, O.C., Emson, C. and Bettess, P.,"A novel boundary infinite element", Int. J. Num. Meth. Eng., Vol.19 (1983), pp.393-404.
56. Reese, L.C., Wang, S.T., Awoshika, K. and Lam, P.H.F.,Documentation of Computer Program Group, Version 3.0, Ensoft, Inc., 1994.
57. Timoshenko, S.T. and Gere, J.M., Theory of Elastic Stability, McGraw-Hill Book Company, Inc., 1961.
58. Drucker, D.C. and Prager, W., "Soil mechanics and plastic analysis of limit design", Quart. Anal. Math., 10, (2), 1952.

Office of Research & Strategic Services
395 John Ireland Blvd., Mail Stop 330
St. Paul, MN 55155-1899

(651) 282-2274